

On Distributed Quantization for Classification

Osama A. Hanna[†], Yahya H. Ezzeldin[†], Tara Sadjadpour[†],

Christina Fragouli[†] and Suhas Diggavi[†]

[†]University of California, Los Angeles

Email: {ohanna, yezzeldin, tsadja, christina.fragouli, suhasdiggavi}@ucla.edu

Abstract

We consider the problem of distributed feature quantization, where the goal is to enable a pretrained classifier at a central node to carry out its classification on features that are gathered from distributed nodes through communication constrained channels. We propose the design of distributed quantization schemes specifically tailored to the classification task: unlike quantization schemes that help the central node reconstruct the original signal as accurately as possible, our focus is not reconstruction accuracy, but instead correct classification. Our work does not make any apriori distributional assumptions on the data, but instead uses training data for the quantizer design. Our main contributions include: we prove NP-hardness of finding optimal quantizers in the general case; we design an optimal scheme for a special case; we propose quantization algorithms, that leverage discrete neural representations and training data, and can be designed in polynomial-time for any number of features, any number of classes, and arbitrary division of features across the distributed nodes. We find that tailoring the quantizers to the classification task can offer significant savings: as compared to alternatives, we can achieve more than a factor of two reduction in terms of the number of bits communicated, for the same classification accuracy.

I. INTRODUCTION

Quantization forms the core of almost all lossy data-compression algorithms, and is widely used to reduce the number of bits required for storage and communication. These schemes optimize a rate-distortion trade-off, where the goal is to represent data using a limited number of bits as precisely as possible. Instead, in this work, we propose distributed quantization schemes tailored to data that are going to be used for classification. That is, we explore the design of

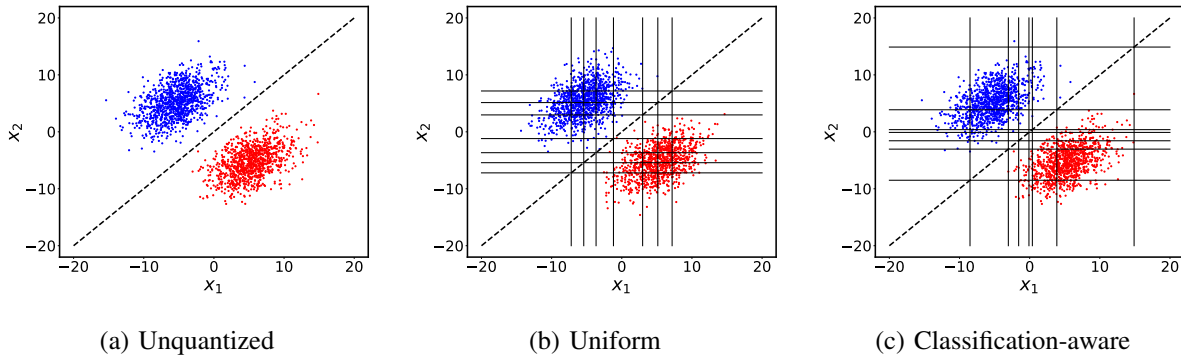


Fig. 1: Example with 2 features and 3 bits/feature: **(a)** Unquantized points separated by a linear classifier; **(b)** Uniform measure quantization; **(c)** Classification-aware quantization.

distributed quantizers for a rate-classification error trade-off: our quantization schemes are not optimized for reconstruction accuracy, but instead correct classification.

Figure 1 illustrates the difference between the two aforementioned approaches. For a given number of bits, we create a corresponding number of quantization regions in the space (3 bits per feature = $2^3 \cdot 2^3 = 64$ regions in our example). Intuitively, for data reconstruction, we want to more finely represent the regions of high signal concentration (Figure 1(b)); for classification, we want to more finely represent areas closer to the classification boundary where errors may happen (Figure 1(c)).

In our work, we aim to design quantizers for the following generic scenario. A central entity has access to a pretrained subdifferentiable classifier (*e.g.*, a multilayer perceptron - MLP [1]) and wishes to apply that classifier on data features collected at K distributed sensor nodes. The communication between the sensors and the central entity comes at a cost (is rate limited), and thus it is expensive to send the measured features with full precision. Instead, each node employs a *distributed single-shot* quantizer¹, independently from other nodes, in order to encode its measurements into bit representations that can be sent to the central entity efficiently as soon as sensed. We emphasize that we do not make any apriori distributional assumptions on the data, as is common in many learning scenarios. Moreover, the data may be heterogeneous, from unknown composite distributions (*e.g.*, multimodal observations of sensors that capture video,

¹Single-shot quantization means that we do not collect samples over time and jointly quantize them. Therefore a set of *local* features observed at a node are quantized together whenever observed; motivated by delay requirement for classification.

sound, and radar signals). We simply use training samples from the data to design the quantizers.

This scenario is motivated by many machine learning applications, that include wireless cyberphysical systems, immersive environments and supported health. For example, in brain-to-computer interface applications, multiple electrodes are placed around the brain to capture brain signals which are used collectively as features to classify in what direction a person is trying to move his hand [2]. Such features need to be quantized at the sensor peripheral nodes, and communicated through rate constrained channels to a central node for processing, so that classification (and decisions based on it) can be done within a reasonable time of sensing.

Our assumption of a pretrained classifier is motivated by the following practical considerations: (i) we may not know the communication channel constraints when designing the classifier and we may want to use the same classifier over systems with different communication channels; (ii) we may not have access to the data used to train the classifier (*e.g.*, we use a pretrained classifier from cloud services such as Google Cloud [3] or Clarifai [4]), but are able to personalize the quantizers leveraging locally available data.

Contributions. We begin our formal study of the problem by proving that in general, it is NP-hard² to design an optimal distributed quantization system tailored for classification of a number of given data points. We also show that the problem is hard to approximate, therefore motivating alternate approaches to the design, and empirical evaluations of proposed techniques.

Given the difficulty of designing the optimal quantization system, we propose a data-based greedy quantization boundary insertion strategy, which we term GBI, which can be used for any type of classifier, any number of features, any number of classes, and arbitrary division of features across the distributed nodes. Operationally, GBI creates rectangular quantization regions by greedily deciding how to divide the training data along each feature. We demonstrate that GBI has quadratic complexity in the number of training samples and linear in the number of features.

To further reduce complexity and capture richer quantization boundaries (beyond rectangular), we propose a (deep) learning based approach to design our quantizers that makes use of the subdifferentiable nature of the classifier employed by the central node. This is inspired by the recent success of learning discrete latent variables [5], [6], joint source channel coding [7] and discrete representations for image compression [8], [9], [10]. Our design can be understood as

²This hardness is in terms of the problem parametrization, *e.g.*, number of training points and the number of features.

a *distributed* discrete neural representation optimized for classification. We leverage the GBI algorithm by making it a module within the discrete neural representation.

Through numerical evaluation, we show that for the same representation budget (number of bits available at sensor nodes for each measurement), we can achieve four folds gains in classification accuracy compared to approaches that try to learn discrete representations aimed directly at reconstruction.

Our main contributions can thus be summarized as follows:

- We prove the NP-hardness and hardness to approximation for designing optimal distributed quantizers for classification.
- We design optimal quantizers for linearly separable data and two features under some structural restrictions.
- We propose a polynomial-complexity greedy quantization algorithm, GBI, optimized for classification, that can be used for any number of features and any classifier.
- We propose a novel distributed discrete neural representation for classification, which can also be combined with GBI.
- When compared with approaches for data reconstruction, we demonstrate benefits of 50% gain in terms of classification accuracy for our proposed quantization approaches, on an sEMG dataset and 300% improvement on the CIFAR10 image dataset.

Paper Organization. Section II, reviews related work; Section III develops the notation and problem framework; Section IV proves the NP-hardness results; Section V, introduces the GBI algorithm; Section VI proposes neural representation schemes; and Section VII presents our numerical evaluation.

II. RELATED WORK

We will give representative examples of related literature to put our work in context, with an organization around specific approaches/problems.

Distributed detection and hypothesis testing. The problem studied in this paper is related to distributed estimation and detection in communication-constrained networks, extensively studied in the literature (see [11], [12] and references therein). Differently from our work, a common assumption is that sensor measurements are independently distributed given the detection hypothesis, and that these conditional distributions are known. In [13], scalar quantization for distributed hypothesis testing was studied, using *known* conditional distribution of features. In contrast to

all these works, we neither assume knowledge of the sensor measurements distribution, nor do we make independence assumptions.

The information theoretic study through error exponents where features are observed at different nodes, is surveyed in [14]. Here, differently from our single-shot setup, an asymptotically long sequence of i.i.d. time samples, from a fixed underlying (unknown) distribution, are jointly compressed to distinguish between two hypotheses (*e.g.*, testing for independence).

There have also been several recent works in information theory and machine learning on distributed probability estimation, property testing and simulation [15], [16], [17]. These works assume that each node observes all features, and has access to independent samples from an unknown underlying distribution. Distinct from this in our setup, each node observes subsets of (non-overlapping) features, *i.e.*, the observations at different nodes are not identically distributed.

Scalar and Vector quantization. In [18], [19], [20] and references therein, a high-rate quantization theory is developed for computing *known* functions from distributed observations, where the source distributions are known. A framework for *centralized* quantizers used for classification can be designed using the learning vector quantization (LVQ) framework [21], [22], where a number of prototype classified vectors are defined and updated to reduce the misclassification error. In contrast, our problem requires decentralized quantization; moreover, the Voronoi tessellation in LVQ may not be decomposable into decision boundaries applicable by distributed quantization.

Multi-terminal function computation. Rate-distortion literature has considered several related problems, where asymptotically large number of samples are jointly represented; moreover these problems assume that distribution of the sources are known. In the classical CEO problem [23], [24], [25], [26], a central node wishes to reconstruct a value from independently corrupted versions measured at distributed sensors. Distributed compression for functional computation with distortion has been studied in [27], [28], [29]. Our work focuses on single-shot quantization for a priori unknown source distributions, without an explicit knowledge of the classifier function.

Model Compression. Quantization is also used in inference tasks for model compression [30], [31], [32], [33], with the goal to simplify implementation and reduce storage. However, differently from our work, the goal is to quantize the model operands rather than focus on distributively quantizing the inputs to the model.

Decision stumps. A closely related algorithm that could be adapted to use for feature quanti-

zation is AdaBoost [34], [35] with decision stumps. In this case, the majority rule on the decision stumps naturally partitions (quantizes) the space based on the number of stumps corresponding to each feature. However, AdaBoost with decision stumps will not necessarily be able to return viable quantizers in all cases. For example, if we consider labeled data points with an XOR pattern in \mathbb{R}^2 (centered at $[-1,-1]$, $[-1,1]$, $[1,-1]$ and $[1,1]$ as shown in Figure 7, Appendix A) then AdaBoost with stumps is not able to represent the XOR pattern in its decision regions [36]. In contrast, it is not difficult to see that two quantization boundaries at $x_1 = 0$ and $x_2 = 0$, respectively, are enough to allow a good classifier to correctly classify the quantized points.

Latent variable models. Perhaps the closest approach to ours, are those of learning latent representations for data reconstruction. In variational autoencoders (VAEs) [37], [38], [39], [40], a continuous latent representation space is learned from the inputs, that can then be used to reconstruct inputs or generate new data that follow the same distribution as the data in the training set. In [5], the authors present a new way of training VAEs to learn discrete latent space representations, which naturally leads to a compression algorithm, since continuous (or full-precision) inputs can be mapped to discrete latent representations typically using fewer bits. In [7], the authors also study the inference of discrete latent variables for joint source and channel coding. In particular, discrete latent variables are learned such that they can be used for compression as in VQ-VAEs; they are also robust to transmission over noisy discrete channels for reconstruction.

A main difference between these implementations and our setup is the *distributed* (decomposable) structure of our quantization system. In addition, it is intuitive to expect that reconstruction may not yield the best classification results; what is perceived by the reconstruction loss as a good approximation of the image might be inappropriate for a classifier as compared to the performance of a classification tailored approach. We explore the latter point empirically in Section VII. Therefore, our work can be thought of as an approach to distributed discrete (neural) representation for classification. Recently, [41] presented a variational approximation to the information bottleneck method [42] to design classifiers. However, differently from our work, it assumed a centralized encoder and continuous latent variables.

III. NOTATION AND PROBLEM FORMULATION

Let \mathcal{X}^n be the n -dimensional space of possible input features (e.g., sensor measurements, images, text, etc.) and \mathcal{Y} be the set of possible classification classes over the space \mathcal{X}^n . We use

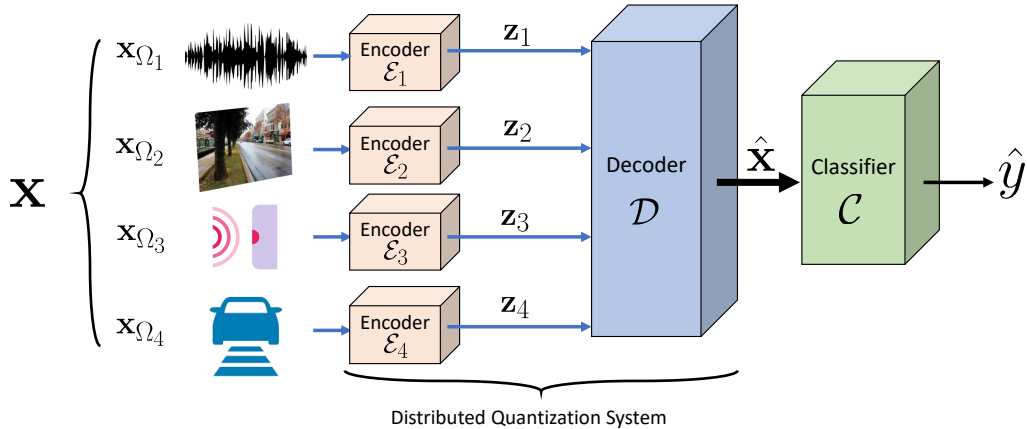


Fig. 2: An example for distributed quantization of features for classification with $K = 4$ nodes.

$\mathbf{x} \in \mathcal{X}^n$ to denote an n -dimensional input and $y(\mathbf{x}) \in \mathcal{Y}$ to denote the class associated with \mathbf{x} .

We consider a scenario where the features of \mathbf{x} are not collected (sensed) all at the same entity but instead at K distributed nodes. An example is shown in Figure 2 for $K = 4$. In particular, node $k \in [1 : K]$ collects the vector of features \mathbf{x}_{Ω_k} indexed by a set $\Omega_k \subseteq [1 : n]$. We assume that the index sets $\{\Omega_k\}_{k=1}^K$ are disjoint and their union is the set $[1 : n]$. We also assume that the feature vector \mathbf{x} is ordered such that $\mathbf{x} = [\mathbf{x}_{\Omega_1}, \mathbf{x}_{\Omega_2}, \dots, \mathbf{x}_{\Omega_K}]$. We denote by \mathcal{X}_{Ω_k} the space defined by the features indexed by Ω_k , with $\mathcal{X}^n = \prod_{k=1}^K \mathcal{X}_{\Omega_k}$.

A central node is interested in classifying the collected input features \mathbf{x} using a pretrained subdifferentiable³ classifier $\mathcal{C}(\cdot)$ where

$$\mathcal{C}(\cdot) : \mathcal{X}^n \rightarrow \mathbb{R}^{|\mathcal{Y}|}, \quad (1)$$

and the output class label $\hat{y}(\mathbf{x})$ is given by

$$\hat{y}(\mathbf{x}) = \arg \max_{i \in [1:|\mathcal{Y}|]} [\mathcal{C}(\mathbf{x})]_i. \quad (2)$$

Note that $\hat{y}(\mathbf{x})$ may be different than the true label $y(\mathbf{x})$. With no communication constraints, node k can perfectly convey \mathbf{x}_{Ω_k} to the central node. Instead, we assume that node k is constrained to use R_k bits (much less than full precision). That is, node k uses a quantizer/encoder \mathcal{E}_k , that

³By “subdifferentiable” classifier, we refer to a classifier that has non-trivial subgradient sets (i.e., not zero everywhere).

takes as input \mathbf{x}_{Ω_k} and produces a discrete representation \mathbf{z}_k from an alphabet \mathcal{M}_k of size at most 2^{R_k} , with

$$\mathbf{z}_k = \mathcal{E}_k(\mathbf{x}_{\Omega_k}) : \mathcal{X}_{\Omega_k} \rightarrow \mathcal{M}_k, \quad \forall k \in [1 : K]. \quad (3)$$

Based on (3), we will denote the preimage of \mathcal{E}_k as

$$\mathcal{E}_k^{-1}(\mathbf{z}_k) = \{\mathbf{x}_{\Omega_k} \in \mathcal{X}_{\Omega_k} | \mathcal{E}_k(\mathbf{x}_{\Omega_k}) = \mathbf{z}_k\}. \quad (4)$$

Note that the computed \mathbf{z}_k depends only on \mathbf{x}_{Ω_k} , the features available at node k . At the central node, in order to apply the pretrained classifier \mathcal{C} , a decoder \mathcal{D} generates $\hat{\mathbf{x}} \in \mathcal{X}^n$ from $\mathbf{z} = [\mathbf{z}_1, \mathbf{z}_2, \dots, \mathbf{z}_K]$ and uses it as the input to the classifier. The end-to-end operation, depicted in Figure 2, is given by (3) and

$$\begin{aligned} \mathbf{z} &= [\mathbf{z}_1, \mathbf{z}_2, \dots, \mathbf{z}_K] \\ \hat{\mathbf{x}} &= \mathcal{D}(\mathbf{z}) : \prod_{k=1}^K \mathcal{M}_k \rightarrow \mathcal{X}^n, \\ \hat{y}(\hat{\mathbf{x}}) &= \arg \max_{i \in [1:|\mathcal{Y}|]} [\mathcal{C}(\hat{\mathbf{x}})]_i. \end{aligned} \quad (5)$$

We refer to a set of encoders $\mathcal{E} = \{\mathcal{E}_k\}_{k=1}^K$ and a decoder \mathcal{D} as a *distributed quantization system* $(\mathcal{E}, \mathcal{D})$. Ideally, we would like to use an $(\mathcal{E}, \mathcal{D})$ system that minimizes the probability of misclassification. That is, the encoders and decoder are the solution of the optimization problem

$$\begin{aligned} &\min_{\mathcal{E}, \mathcal{D}: |\mathcal{M}_k| \leq 2^{R_k}} \mathbb{E}_{\mathbf{x}, y(\mathbf{x}) \sim p(\mathbf{x}, y(\mathbf{x}))} [\mathbb{I}(\hat{y}(\hat{\mathbf{x}}) \neq y(\mathbf{x}))] \\ &= \min_{\mathcal{E}, \mathcal{D}: |\mathcal{M}_k| \leq 2^{R_k}} \mathbb{E}_{\mathbf{x}, y(\mathbf{x}) \sim p(\mathbf{x}, y(\mathbf{x}))} [\mathbb{I}(\hat{y}(\mathcal{D}(\mathcal{E}(\mathbf{x}))) \neq y(\mathbf{x}))], \end{aligned} \quad (6)$$

where: (i) $p(\mathbf{x}, y(\mathbf{x}))$ is the input data distribution; (ii) $\hat{y}(\hat{\mathbf{x}})$ and $\hat{\mathbf{x}}$ are obtained from \mathbf{x} using (3) and (5); and (iii) we used $\mathbf{z} = \mathcal{E}(\mathbf{x})$ for brevity.

However, in this paper we assume that the distribution $p(\mathbf{x}, y(\mathbf{x}))$ is not known: instead, we are given a dataset $\mathcal{T} = \{(\mathbf{x}^{(i)}, y(\mathbf{x}^{(i)}))\}_{i=1}^N$ which contains N independent samples drawn from $p(\mathbf{x}, y(\mathbf{x}))$. Thus, we can only empirically approximate the expectation in (6) using the dataset \mathcal{T} , and hence, our objective is to minimize the *misclassification loss* $\mathcal{L}(\mathcal{E}, \mathcal{D}, \mathcal{T})$, calculated as

$$\mathcal{L}(\mathcal{E}, \mathcal{D}, \mathcal{T}) = \frac{1}{N} \sum_{i=1}^N [\mathbb{I}(\hat{y}(\hat{\mathbf{x}}^{(i)}) \neq y(\mathbf{x}^{(i)}))]. \quad (7)$$

In the rest of the paper, we will say that a distributed quantization system $(\mathcal{E}, \mathcal{D})$ is *optimal*, if the encoders $\mathcal{E} = \{\mathcal{E}_k\}_{k=1}^K$ and the decoder \mathcal{D} are an optimal solution of the problem

$$\min_{\mathcal{E}, \mathcal{D}: |\mathcal{M}_k| \leq 2^{R_k}} \mathcal{L}(\mathcal{E}, \mathcal{D}, \mathcal{T}). \quad (8)$$

Remark 1. Note that in (7), given a labeled dataset \mathcal{T} , our objective is to minimize the empirical probability of misclassifying the data points $\mathbf{x}^{(i)}$ after quantization. Instead, if we are given a local dataset of unlabeled data points, $\mathcal{T}_u = \{\mathbf{x}^{(i)}\}_{i=1}^N$, we could create a labeled dataset, $\widehat{\mathcal{T}} = \{(\mathbf{x}^{(i)}, \widehat{y}(\mathbf{x}))\}_{i=1}^N$, by applying the pretrained classifier \mathcal{C} on the local unlabeled data \mathcal{T}_u . We can then apply (7) - and the logic in the remainder of the paper - on the data $\widehat{\mathcal{T}} = \{(\mathbf{x}^{(i)}, \widehat{y}(\mathbf{x}))\}_{i=1}^N$. In this case, our objective is equivalent to keeping the classifier output consistent before and after applying the distributed quantization system.

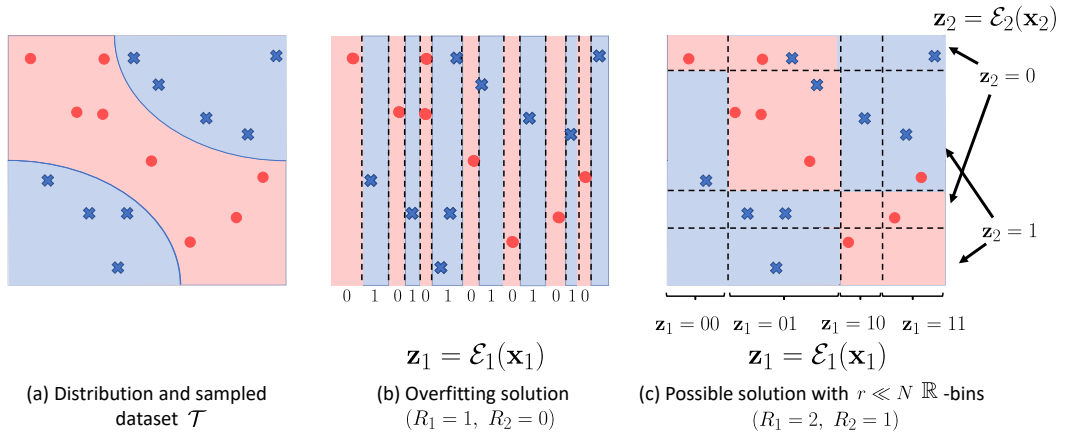


Fig. 3: Quantization example.

Remark 2. With no structural restrictions on the encoders \mathcal{E} , it is possible to achieve $\mathcal{L}(\mathcal{E}, \mathcal{D}, \mathcal{T}) = 0$ almost-surely through over-fitting. For instance, if the distribution $p(\mathbf{x})$ is a continuous distribution, the probability that two data points have the same value for \mathbf{x}_{Ω_k} is zero for any k . Thus, we can consider for example the first node ($k = 1$), and partition the space of \mathbf{x}_{Ω_1} into N disjoint regions such that each region contains only one training data point. Then, for each region, the encoder function $\mathcal{E}_1(\cdot)$ at node 1 can directly output the class $y(\mathbf{x}^{(i)})$ of the data point $\mathbf{x}^{(i)}$ contained in that region, then the decoder outputs a data point that is classified by the classifier to be $y(\mathbf{x}^{(i)})$. This requires only $\log_2(|\mathcal{Y}|)$ bits. Hence, the rates $[R_1, \dots, R_K] = [\log_2(|\mathcal{Y}|), 0, \dots, 0]$

are sufficient to achieve $\mathcal{L}(\mathcal{E}, \mathcal{D}, \mathcal{T})=0$. Although such a quantization scheme will have zero loss when evaluated on the dataset \mathcal{T} , it would obviously handle out of sample points very poorly.

To avoid this, we restrict the preimage $\mathcal{E}_k^{-1}(\mathbf{z}_k)$ to be the union of at most r \mathcal{X}_{Ω_k} -bins, which are defined below.

Definition 1 (\mathcal{S} -bin). We say that the set $\mathcal{A} \subseteq \mathcal{S}$ is an \mathcal{S} -bin if \mathcal{A} is path-connected [43] in \mathcal{S} . A set \mathcal{A} is path-connected if and only if for every pair of points $a, b \in \mathcal{A}$, there exists a path that connects a, b which completely lies inside \mathcal{A} . More formally, a set \mathcal{A} is said to be path-connected if and only if for every pair of points $a, b \in \mathcal{A}$, there exists a continuous function $f : [0, 1] \rightarrow \mathcal{A}$ such that $f(0) = a$ and $f(1) = b$ [43].

By restricting the preimage of $\mathcal{E}_k^{-1}(\mathbf{z}_k)$ to $r \ll N$ \mathcal{X}_{Ω_k} -bins, we force \mathcal{E}_k to assign the same \mathbf{z}_k to a limited number of path-connected regions (earlier, these could be as many as the number of data points from the same class). By doing so, the solution discussed above (where a single encoder can fully carry the burden of classifying the data points) is eliminated.

We illustrate how the introduction of this restriction can reduce overfitting in the learned quantization system through the example shown in Figure 3. Figure 3(a) depicts the underlying true class function $y(\mathbf{x})$ through colored regions of \mathbb{R}^2 and the sampled dataset \mathcal{T} as points scattered in the plot. Figure 3(b) shows how an overfitting quantization system (as described in Remark 2) using only \mathbf{x}_1 would approximate the underlying class function y . Note that, although the resulting system provides poor approximation, it classifies the dataset points perfectly (given by the background color in each region). Finally, Figure 3(c) shows an example where each encoder \mathcal{E}_k assigns at most 2 \mathbb{R} -bins to the same \mathbf{z}_k . It is not difficult to see that although the illustrated quantization system does misclassify some points in the dataset (decision given by the background in each region), it gives a better approximation of $y(\mathbf{x})$ outside the given dataset compared to the design in 3(b).

A summary of the notation used throughout the paper is given in Table I.

IV. ON THE COMPLEXITY OF FINDING AN OPTIMAL DISTRIBUTED QUANTIZATION SYSTEM

In this section we study the complexity of finding an optimal quantization system $(\mathcal{E}, \mathcal{D})$ that minimizes the loss in (8) over the dataset \mathcal{T} . We first start by describing how to find an optimal decoder \mathcal{D} assuming that the optimal encoders $\mathcal{E}^* = \{\mathcal{E}_k^*\}_{k=1}^K$ are given. We then discuss the

Symbol	Description	Symbol	Description
K	Number of distributed sensing nodes	\mathcal{M}_k	Set of possible values for \mathbf{z}_k (def. (3))
n	Number of features of data point \mathbf{x}	\mathbf{z}	Collection of encoder outputs $[\mathbf{z}_1, \mathbf{z}_2, \dots, \mathbf{z}_K]$ (def. (5))
\mathcal{Y}	Set of possible classes	\mathcal{M}	Set of possible values for \mathbf{z} (def. (5))
y	True class label of data point \mathbf{x}	$\hat{\mathbf{x}}$	Reconstructed input from \mathbf{z} using \mathcal{D} (def. (5))
Ω_k	Set of features at node k	$\mathcal{L}(\mathcal{E}, \mathcal{D}, \mathcal{T})$	Empirical misclassification loss (def. (7))
R_k	Number of bits/data point at node k	\mathcal{S} -bin	Path-connected subset of \mathcal{S} (def. Definition 1)
\mathcal{C}	Pretrained classifier (def. (1))	p_e	Misclassification loss threshold (def. Lemma 2)
\hat{y}	Output class by classifier \mathcal{C} (def. (2))	d	Set of boundaries used in optimal on-the-line quantizer
\mathcal{E}_k	Encoder at node k (def. (3))	$f_k(\cdot; \theta_k)$	Neural network of neural driven encoder \mathcal{E}_k
\mathcal{E}_k^{-1}	Preimage of \mathcal{E}_k (def. (4))	\mathbb{R}^{m_k}	Output space of neural encoder f_k (def. (15))
\mathcal{E}	Collection of encoders $\{\mathcal{E}_k\}_{k=1}^K$	\mathcal{Q}_k	Quantizer of neural driven encoder \mathcal{E}_k (def. (15))
\mathcal{D}	Decoder at central node (def. (5))	\mathcal{G}	Initial mapping of neural driven decoder \mathcal{D} (def. (16))
\mathcal{T}	Training dataset $\{(\mathbf{x}^{(i)}, y(\mathbf{x}^{(i)}))\}_{i=1}^N$	$g(\cdot; \phi)$	Neural network of neural driven decoder \mathcal{D} (def. (16))
N	Number of data points in \mathcal{T}	\mathcal{L}^c	Misclassification loss for neural based approach (def. (18))
\mathbf{z}_k	Output of encoder \mathcal{E}_k (def. (3))	\mathcal{L}^q	Quantization loss for neural based approach (def. (20))

TABLE I: Notation used throughout the paper.

complexity of finding optimal encoders and show that the problem is NP-hard in all cases but one. For the case where the problem is not NP-hard, we propose a polynomial-time algorithm to find the optimal quantization system (encoders/decoder) under some structural restrictions on the encoders.

A. Optimal decoder

Assuming that the optimal encoders \mathcal{E}^* are given, we are interested in a decoder \mathcal{D}^* that minimizes the misclassification loss in (8). For brevity, let us denote the set of all possible encoded values $\mathbf{z} = \mathcal{E}^*(\mathbf{x})$ as \mathcal{M} , i.e.,

$$\mathbf{z} \in \mathcal{M}, \quad \text{where} \quad \mathcal{M} = \prod_{k=1}^K \mathcal{M}_k. \quad (9)$$

The operation of the optimal decoder is described in the following lemma.

Lemma 1. *For given fixed encoders \mathcal{E}^* , the optimal decoder \mathcal{D}^* is defined by*

$$\mathcal{D}^*(\mathbf{z}) = \hat{\mathbf{x}} \quad \text{s.t.} \quad \hat{y}(\hat{\mathbf{x}}) = \arg \max_{c \in \mathcal{Y}} \sum_{i: \mathcal{E}^*(\mathbf{x}^{(i)})=\mathbf{z}} \mathbb{I}[y(\mathbf{x}^{(i)}) = c], \quad (10)$$

where \hat{y} , defined in (2), is the label output by the classifier \mathcal{C} for $\hat{\mathbf{x}}$.

Proof. The misclassification loss in (7) can be rewritten as

$$\mathcal{L}(\mathcal{E}^*, \mathcal{D}, \mathcal{T}) = \frac{1}{N} \sum_{\mathbf{z} \in \mathcal{M}} \sum_{i: \mathcal{E}^*(\mathbf{x}^{(i)}) = \mathbf{z}} \mathbb{I} [y(\mathbf{x}^{(i)}) \neq \hat{y}(\mathcal{D}(\mathbf{z}))], \quad (11)$$

where $\hat{y}(\mathcal{D}(\mathbf{z}))$ is obtained by (5). Since for a fixed \mathbf{z} , $\mathcal{D}(\mathbf{z})$ only affects one term in the outer summation in (11), each of the outer summation terms can be independently minimized by choosing $\mathcal{D}^*(\mathbf{z})$ to be a point $\hat{\mathbf{x}} \in \mathcal{X}^n$ satisfying

$$\begin{aligned} \hat{y}(\hat{\mathbf{x}}) &= \arg \min_{c \in \mathcal{Y}} \sum_{i: \mathcal{E}^*(\mathbf{x}^{(i)}) = \mathbf{z}} \mathbb{I} [y(\mathbf{x}^{(i)}) \neq c] = \arg \min_{c \in \mathcal{Y}} \left(N - \sum_{i: \mathcal{E}^*(\mathbf{x}^{(i)}) = \mathbf{z}} \mathbb{I} [y(\mathbf{x}^{(i)}) = c] \right) \\ &= \arg \max_{c \in \mathcal{Y}} \sum_{i: \mathcal{E}^*(\mathbf{x}^{(i)}) = \mathbf{z}} \mathbb{I} [y(\mathbf{x}^{(i)}) = c]. \end{aligned} \quad (12)$$

□

That is, $\hat{\mathbf{x}} = \mathcal{D}^*(\mathbf{z})$ can be any point in \mathcal{X}^n such that $\hat{y}(\hat{\mathbf{x}})$ (the decision of classifier \mathcal{C} for $\hat{\mathbf{x}}$) is the majority true label $y(\mathbf{x})$ among the points of the dataset \mathcal{T} that fall in $\mathcal{E}^{-1}(\mathbf{z})$. For instance, in the example shown in Figure 3, if $\mathcal{E}^{\star-1}(\mathbf{z})$ has one “x” (blue) and two “o” (red) training points, any point that the classifier \mathcal{C} would classify to be “o” (red) can be selected as $\hat{\mathbf{x}} = \mathcal{D}^*(\mathbf{z})$. Thus, the optimal decoder \mathcal{D}^* manipulates the classifier \mathcal{C} to output a classification that best serves the loss function in (11).

With the optimal decoder in mind, we are now ready to discuss the hardness of the problem of finding the optimal encoders \mathcal{E} in the following subsection.

B. Hardness of finding an optimal quantizer

Given a training dataset $\mathcal{T} = \{(\mathbf{x}^{(i)}, y^{(i)})\}_{i=1}^N$, our goal is to design an *optimal* distributed quantization system $(\mathcal{E}, \mathcal{D})$ which minimizes the misclassification loss in (7) for a given communication budget of R_k bits per data point at each node k . We study four different cases of the problem:

- (P1)** For number of features $n > 1$, number of classes $|\mathcal{Y}| > 1$, dataset $\mathcal{T} = \{(\mathbf{x}^{(i)}, y^{(i)})\}_{i=1}^N$ and given $\{R_k\}_{k=1}^K$: find the optimal $(\mathcal{E}, \mathcal{D})$ that minimizes the misclassification loss $\mathcal{L}(\mathcal{E}, \mathcal{D}, \mathcal{T})$, assuming that $\mathcal{E}_k^{-1}(\mathbf{z}_k)$ is the union of $r < N$ \mathcal{X}_{Ω_k} -bins.
- (P2)** The restriction of problem **(P1)** to the case of linearly separable data.
- (P3)** The restriction of problem **(P1)** to the case where $\mathcal{E}_k^{-1}(\mathbf{z}_k)$ is a single \mathcal{X}_{Ω_k} -bin.
- (P4)** The restriction of problem **(P3)** to the case of linearly separable data.

Next, we prove that the first three problems for $n > 1$ and the last problem for $n > 2$ are NP-hard and also prove their hardness of approximation. In the general case, as a result of the hardness and hardness of approximation, we focus on finding heuristic approaches to find a good distributed quantization solution that may not necessarily be optimal.

Remark 3. For problem **(P4)**, we prove the hardness results for number of features $n \geq 3$. In the next subsection, we introduce optimal polynomial-time algorithm for the case $n = 2$ under some structural restrictions on the encoders.

For all the problems, in order to prove the goal results, it is sufficient to consider prototype settings with predefined number of features n , number of classes $|\mathcal{Y}|$, number of nodes K , and communication budget $\{R_k\}_{k=1}^K$ and allow the size N of the dataset \mathcal{T} to grow. It follows that the general problems, which are expansions of these prototype problems, are also NP-hard. In particular, in all cases, we assume that each distributed node quantizes only one feature (i.e., $n = K$) and the number of classes $|\mathcal{Y}| = 2$. The remaining parameters are defined below for each problem

- **(P1)** & **(P2)** : $n = K = 2$, finite R_1 and $R_2 \rightarrow \infty$;
 - **(P3)** : $n = K = 2$, finite $R_1 = R_2$;
 - **(P4)** : $n = K = 3$, $R_3 = 0$ and finite $R_1 = R_2$.
- (13)

We start by showing that, under polynomial-time reductions, the problem of finding the optimal quantization system in **(P1)**- **(P4)** with the aforementioned parameters is equivalent to finding the minimum number of bits $\{R_k\}_{k=1}^K$ required for a particular fixed misclassification error p_e . In particular, the equivalence is summarized in the following lemma.

Lemma 2. *For a fixed $p_e \in [0, 1]$ and number of classes $|\mathcal{Y}| = 2$: the problems **(P1)** - **(P4)** with parameters in (13) are equivalent to **(P1')** - **(P4')** below under polynomial-time reductions:*

- (P1')** *For number of features $n = 2$, $R_2 \rightarrow \infty$, finding the minimum R_1 for which $\mathcal{L}(\mathcal{E}, \mathcal{D}, \mathcal{T}) < p_e$, assuming that $\mathcal{E}_k^{-1}(\mathbf{z}_k)$ is the union of $r < N$ \mathcal{X}_{Ω_k} -bins.*
- (P2')** *The restriction of problem **(P1')** to the case of linearly separable data.*
- (P3')** *For number of features $n = 2$, finding the minimum $R_1 = R_2$ for which $\mathcal{L}(\mathcal{E}, \mathcal{D}, \mathcal{T}) < p_e$, assuming that $\mathcal{E}_k^{-1}(\mathbf{z}_k)$ is a single \mathcal{X}_{Ω_k} -bin.*

(P4') For number of features $n=3$, $R_3=0$, finding the minimum $R_1 = R_2$ for which $\mathcal{L}(\mathcal{E}, \mathcal{D}, \mathcal{T}) < p_e$ for the case of linearly separable data, assuming that $\mathcal{E}_k^{-1}(\mathbf{z}_k)$ is a single \mathcal{X}_{Ω_k} -bin.

Proof. The proof is based on the observation that the loss $\mathcal{L}(\mathcal{E}, \mathcal{D}, \mathcal{T})$ can only take one of the $N + 1$ values: $0, \frac{1}{N}, \frac{2}{N}, \dots, \frac{N}{N}$, and 2^{R_1} can only take values in $[1 : N]$. Hence, if we have a polynomial-time algorithm which solves problem **(P1)** in $O(f(N))$, then we can answer the mentioned question in $O(Nf(N))$ by finding the minimum loss $\forall R_1 \in [\log_2(1), \log_2(2), \dots, \log_2(N)]$ and pick the smallest R_1 for which the minimum achieved loss is less than p_e . Similarly, if we have a polynomial-time algorithm that answers this question, then we can solve problem **(P1)** in polynomial time. Hence, **(P1')** and problem **(P1)** are equivalent under polynomial-time reduction. Following the same logic, problem **(P2)** - **(P4)** are equivalent to **(P2')** - **(P4')**. \square

Based on Lemma 2, the hardness results can now be proved by working directly with **(P1')** - **(P4')**. In particular, these problems are NP-hard as stated in the following theorem.

Theorem 1. For a fixed $p_e \in [0, 1]$ and number of classes $|\mathcal{Y}| = 2$, the problems **(P1')** - **(P4')** are NP-hard. Moreover, we have that

- Approximating 2^{R_k} in problems **(P1')**, **(P2')** within $O(N^{1-\epsilon})$ is NP-hard $\forall \epsilon > 0$.
- Approximating 2^{R_k} in problems **(P3')**, **(P4')** within $O(N^{\frac{1}{2}-\epsilon})$ is NP-hard $\forall \epsilon > 0$ assuming the Small Set Expansion Hypothesis (SSEH) and that $NP \not\subseteq BPP$.

Proof. We prove the results for each problem by reduction from an NP-Complete problem. In particular, we prove the result for **(P1')**, **(P2')** by reduction from the vertex coloring problem, and for **(P3')**, **(P4')** by reduction from the maximum balanced biclique problem. The proof is delegated to Appendix B. \square

C. Optimal Quantizer for Linear Classifiers in 2D

In the previous section, we proved that, for problem **(P4)** when $n > 3$, it is NP-hard to find an optimal quantization system. In this subsection, we propose an optimal polynomial-time algorithm for problem **(P4)** when the number of features is $n = 2$ under some structural restrictions on the encoders. Specifically, we consider a system with two distributed nodes. Each node $k \in [1 : 2]$, observes one feature x_k , and aims to quantize x_k using R bits. We assume that we have two classes ($|\mathcal{Y}| = 2$) to distinguish among and that the data is linearly separable, namely, \mathcal{C} is a linear classifier with output $\hat{y}(\mathbf{x}) = y(\mathbf{x})$. Moreover, without loss of generality, we

assume that the features are scaled and translated such that the line $x_1 = x_2$ separates the data. This transformation can be performed during encoding at each distributed node and reverted in the decoder \mathcal{D} at the central node. Note that in this case, since $\mathcal{X}_{\Omega_k} = \mathbb{R}, \forall k \in [1 : 2]$ and an

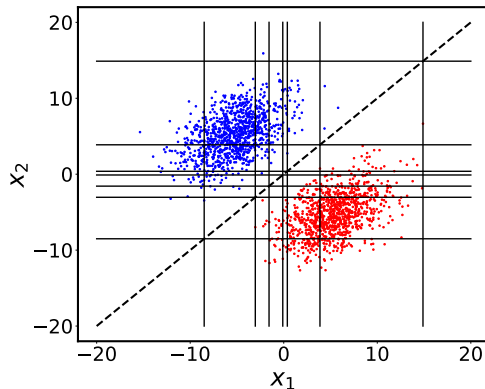


Fig. 4: Example of on-the-line quantizer, where boundaries for x_1 and x_2 intersect along the $x_1 = x_2$ line (45° line).

\mathbb{R} -bin is an interval $[a, b]$ for some a, b , then the encoder/quantizer at node k divides $\mathcal{X}_{\Omega_k} = \mathbb{R}$ into 2^R intervals by introducing the quantization boundaries $(d_{k,1}, \dots, d_{k,2^R-1})$. We here further restrict our attention to the class of **on-the-line** quantizers, where the horizontal and vertical lines defining $d_{k,i}$ meet along the line $x_1 = x_2$ (as in Figure 4). In other words, nodes 1 and 2 use a common encoder design $\mathcal{E}_1 = \mathcal{E}_2$. This implies that $d_{0,k} = d_{1,k} = d_k$, and thus we simply need to find the $2^R - 1$ quantization boundaries (d_1, \dots, d_{2^R-1}) .

Remark 4. Note that although d_k can take any value in \mathbb{R} , only $2N$ values can make a difference in the misclassification loss in (7): the $2N$ values corresponding to either coordinate of the training data points $\{\mathbf{x} | (\mathbf{x}, y(\mathbf{x})) \in \mathcal{T}\}$. Indeed, these are the only boundaries that can change the bin to which a training point belongs⁴.

To find the on-the-line optimal quantizer, we could simply do an exhaustive search over all possible $2N$ values (recall Remark 4) that each of the boundaries d_k can take which costs a complexity of $O\left(\binom{2N}{2^R}\right)$, which is not efficient. Instead, we use a recursive approach, that is based on the following two key observations.

⁴If a point lies on a boundary, we assume it belongs to the bin preceding that boundary.

Remark 5. The encoders/quantizers $\mathcal{E}_1, \mathcal{E}_2$ decompose \mathbb{R}^2 into 2^{2R} \mathbb{R}^2 -bins. However, since the data points are assumed to be linearly separable by the line $x_1 = x_2$, then we only need to consider the \mathbb{R}^2 -bins crossed by $x_1 = x_2$ as the sources of misclassification. In particular, any other \mathbb{R}^2 -bin is completely populated by data points from the same class.

Remark 6. Assume that a vector \mathbf{s} lists the $2N$ possible boundary values in ascending order, i.e., $s_j \leq s_i$ for all $j \leq i \leq 2N$. Let \mathcal{T}_{s_i} denote the subset of the dataset \mathcal{T} such that both coordinates of \mathbf{x} are upper bounded by s_i , i.e.,

$$\mathcal{T}_{s_i} = \{(\mathbf{x}, y(\mathbf{x})) \in \mathcal{T} | x_1, x_2 \leq s_i\}, \quad \forall i \in [1 : 2N]. \quad (14)$$

Note that $\mathcal{T}_{s_j} \subseteq \mathcal{T}_{s_i}, \forall i < j$ and that $\mathcal{T}_{s_{2N}} = \mathcal{T}$. Then, the optimal quantizer with b boundaries on \mathcal{T}_{s_i} shares $b - 1$ boundaries with the optimal quantizer with $b - 1$ boundaries on \mathcal{T}_{s_j} for some $j < i$.

Remark 6 is restated and proved in Appendix C. Observations in Remark 5 and Remark 6 lead to a polynomial-time dynamic-programming algorithm to design the optimal quantization boundaries (d_1, \dots, d_{2^R-1}) .

The algorithm's pseudo code is given in Algorithm 1 and implements the following logic: Given an ordered list of the possible $2N$ boundary values \mathbf{s} , let $E(s_i, b)$ be the minimum number of misclassified points over the dataset subset \mathcal{T}_{s_i} when using b boundaries and $A(s_i, b)$ be the set of boundaries that achieve this minimum loss. Then in each iteration $i \in [1 : 2N]$:

- 1) Find $E(s_i, b), \forall b \in [1 : 2^R - 1]$ by trying to augment $A(s_j, b - 1), \forall j < i$ with one extra boundary at s_j (Remark 6). The additional number of misclassified points is only a result of the points in $\{(\mathbf{x}, y(\mathbf{x})) \in \mathcal{T} | s_j < x_1 \leq s_i, s_j < x_2 \leq s_i\}$ (Remark 5);
- 2) Retain the best augmentation $A(s_i, b)$ to be used in the following iteration;
- 3) After $2N$ iteration, the optimal quantization boundaries are stored in $A(s_{2N}, 2^R - 1)$.

In the worst case the algorithm does $2N \times 2^R$ iterations over the whole dataset \mathcal{T} resulting in a time-complexity of $O(N^2 2^R)$. The optimality of Algorithm 1 is proved in Appendix C as a consequence of proving the observation in Remark 6.

In the following section, we introduce an approach for designing the encoders and decoder in a more general setting, i.e., when the data points are not necessarily linearly separable and the number of nodes and features are greater than or equal to 2.

Algorithm 1 Optimal on-the-line quantizer for linearly separable data in \mathbb{R}^2

Input: (a) Training set $\{(\mathbf{x}^{(i)}, y(\mathbf{x}^{(i)}))\}_{i=1}^N$; (b) Quantization bits/feature R ; (c) Ordered set \mathbf{s} of potential boundary values.

By $\mathbf{x} \preceq p$ we express that all elements in \mathbf{x} are less than p ; $p \prec \mathbf{x}$ means they all exceed p

Output: Quantization boundaries $(d_1, d_2, \dots, d_{2^R-1})$ to use for features x_1 and x_2

Initialize:

$$E(s, 0) \leftarrow \min_{c \in \{1, 2\}} |\{j | \mathbf{x}^{(j)} \preceq s, y^{(j)} = c\}| \quad \text{for } s \in \mathbf{s}$$

for $i \in [1 : |\mathbf{s}|]$ **do**

for $b \in [1 : 2^R - 1]$ **do**

$$E(s_i, b) \leftarrow \min_{\ell < i} \left\{ E(s_\ell, b - 1) + \min_{c \in \{1, 2\}} |\{j | s_\ell \prec \mathbf{x}^{(j)} \preceq s_i, y^{(j)} = c\}| \right\}$$

$\ell^* \leftarrow$ index ℓ that gave the minimum value for $E(s_i, b)$ in the previous expression

$$A(s_i, b) \leftarrow A(s_{\ell^*}, b - 1) \cup \{s_{\ell^*}\}$$

return $A(s_{|\mathbf{s}|}, 2^R - 1)$

V. GREEDY BOUNDARY INSERTION (GBI) QUANTIZER

We refer the reader to Table I for the system notation used in this section. Here, we propose our Greedy Boundary Insertion (GBI) algorithm to design encoders/quantizers $\mathcal{E}_k, \forall k \in [1 : K]$, that can be executed in polynomial-time in the dataset size N and the number of features n for any number of classes. For the decoder \mathcal{D} , we use the optimal decoder derived in Section IV-A. GBI extends the intuition in the observations in Subsection IV-C to a more general case, where the classifier is arbitrary, and where each distributed node k observes Ω_k features and can have arbitrary rate R_k . We design encoders/quantizers such that $\mathcal{E}_k^{-1}(\mathbf{z}_k)$ (see (4)) is a single \mathcal{X}_{Ω_k} -bin. Note that, since we are not constrained to use the same boundaries for each feature as in the on-the-line case, it is sufficient to consider N possible boundary values per feature, the values taken at that feature by the N training points.

The logic behind GBI is as follows. GBI iteratively adds quantization boundaries selected greedily: at each iteration it selects to add one of the possible N boundaries to one of the n features, the one that minimizes the misclassification loss in (8) given the choice of boundaries

in the previous iterations⁵. A feature i can accept a new boundary, if $i \in \Omega_k$ for some node k and introducing a new boundary for feature i does not cause node k to have more than $2^{R_k} \mathbb{R}^{|\Omega_k|}$ -bins. The algorithm terminates when none of the features can accept a new boundary. If two or more possible boundaries lead to the same loss (something that happened surprisingly often in our experiments), then instead of breaking ties at random, it makes a significant performance difference to break ties by using a non-linear criterion. This criterion penalizes a boundary that leaves \mathbb{R}^n -bins with high individual misclassification to correct classification ratio. This is discussed in more detail in Appendix D.

The pseudo code for GBI is presented in Algorithm 2. The losses computed in Algorithm 2 assume that the optimal decoder (defined by Lemma 1) for the designed encoders is used.

Using this notation, the pseudocode for GBI is presented in Algorithm 2.

Complexity of GBI. At each iteration of the algorithm, we compute the reduction in misclassification error associated with every potential boundary and pick the boundary with the most reduction. This involves $O(N)$ operations per boundary. Thus to add a single boundary, $O(nN^2)$ operations are needed in the worst-case. This results in time-complexity of $O(nN^2 2^{R_{\max}})$, where $R_{\max} = \max_k R_k$. Recall that our focus is on cases where the number of bits used are much lower than required for full precision (32 bits). As a result, the contribution of R_k in the complexity term can be subsumed into the notation $O(nN^2)$.

Remark 7. Despite the fact that GBI is a polynomial-time algorithm, we are interested in approaches with linear complexity in N , as the number of available data points (as well as features) in a dataset can be large. To overcome the effect of quadratic complexity in N , GBI can be applied stochastically by randomly sampling a subset of the dataset \mathcal{T} to use at each iteration (instead of evaluating the decrease in misclassification over the whole dataset \mathcal{T}).

Remark 8. A possible drawback of GBI is that boundaries are directly introduced on the native features without transformation. Thus, as aforementioned, the resulting encoder \mathcal{E}_k at node k would always have a rectangular grid structure where each area in the grid would be assigned to some \mathbf{z}_k . It is not difficult to see that allowing a transformation on the features available at node k (i.e., Ω_k), can allow more elaborate encoder designs. We study how to design such

⁵Since GBI adds a boundary for one feature at a time, instead of a function of the features \mathbf{x}_{Ω_k} , we end up with an encoder of the form of a rectangular-grid, where each region is assigned to a value of \mathbf{z}_k .

Algorithm 2 GBI Algorithm

Variables:

$\{\mathbf{d}\}_{f=1}^n$: Boundaries for feature $f \in [1 : n]$;

B_k : Number of \mathbb{R}^{Ω_k} -bins used by node $k \in [1:K]$ using boundaries $\{\mathbf{d}_f\}_{f \in \Omega_k}$;

$\mathcal{L}(\mathbf{d}_1, \dots, \mathbf{d}_n)$: misclassification loss (defined in (6)) using encoders defined by $\{\mathbf{d}\}_{f=1}^n$;

$\Delta_k(f, \{\mathbf{d}_j\}_{j \in \Omega_k})$: Increase in B_k , if a new boundary is introduced for feature f .

Input: (a) Training set $\{(\mathbf{x}^{(i)}, y(\mathbf{x}^{(i)}))\}_{i=1}^N$; (b) Quantization bits/node $R_k, \forall k \in [1 : K]$.

Output: Quantization boundaries $\mathbf{d}_f = \{d_{f,1}, d_{f,2}, \dots\}, \forall f \in [1 : n]$

Initialize:

1) List \mathbf{s}_f of potential boundaries for feature f from the training set, i.e., $\mathbf{s}_f \leftarrow \{x_f^{(i)}\}_{i=1}^N$

2) Number of current bins in node k , $B_k = 0$, boundaries $\mathbf{d}_f = \phi$ for each feature f

while $\exists k : B_k + \min_{f \in \Omega_k} \Delta_k(f, \{\mathbf{d}_j\}_{j \in \Omega_k}) \leq 2^{R_k}$ **do**

- Among all k satisfying condition above, find $\hat{f} \in \Omega_k, \hat{d} \in \mathbf{s}_{\hat{f}}$ that minimizes

$$\mathcal{L}(\mathbf{d}_1, \dots, \mathbf{d}_{\hat{f}} \cup \{\hat{d}\}, \dots, \mathbf{d}_n)$$

- If there are more than one pair (\hat{d}, \hat{f}) achieving the same minimum objective value, we break ties using a non-linear criterion (Appendix D)

Update:

$$\mathbf{d}_{\hat{f}} \leftarrow \mathbf{d}_{\hat{f}} \cup \{\hat{d}\}$$

$$B_k \leftarrow B_k + \Delta_k(\hat{f}, \{\mathbf{d}_j\}_{j \in \Omega_k}), \quad \text{where } \hat{f} \in \Omega_k$$

a transformation before applying GBI as part of the deep learning approach proposed in the following section.

VI. DISTRIBUTED QUANTIZATION FOR CLASSIFICATION TASKS USING NEURAL REPRESENTATIONS

In this section, we explore a learning based approach for the distributed quantization problem introduced in Section III. We consider a quantization system where the encoders $\{\mathcal{E}_k\}_{k=1}^K$ and decoder \mathcal{D} are neural networks, followed by a pretrained classifier \mathcal{C} that is subdifferentiable.

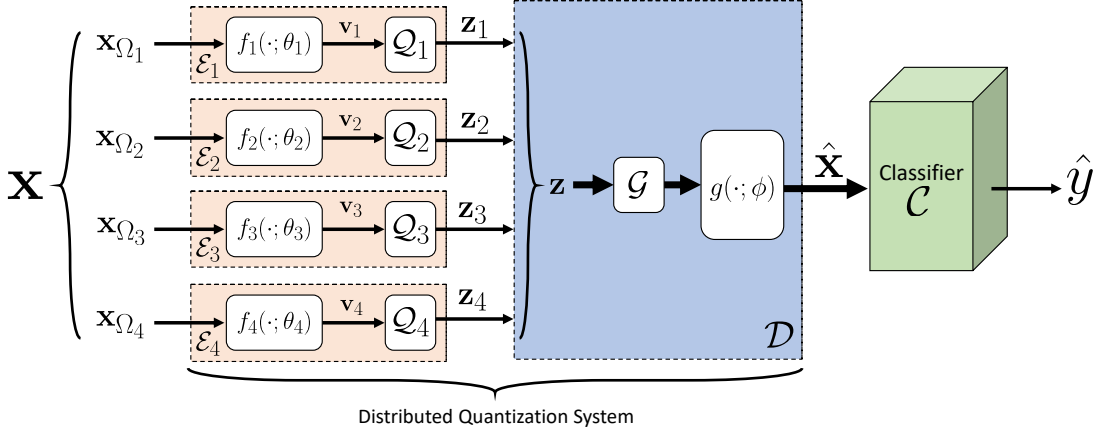


Fig. 5: An example of the different components of encoders and decoders in the distributed quantization system for $K = 4$ nodes.

The structure of the encoders and decoder is shown in Figure 5. In particular, the encoder $\mathcal{E}_k(\cdot)$ is decomposed into a neural network parameterized by θ_k , which implements a function $f_k(\cdot; \theta_k) : \mathcal{X}_{\Omega_k} \rightarrow \mathbb{R}^{m_k}$, followed by a quantizer $\mathcal{Q}_k : \mathbb{R}^{m_k} \rightarrow \mathcal{M}_k$ that maps the output of the neural network to a discrete set $\mathcal{M}_k \subseteq \mathbb{R}^{m_k}$ of size at most 2^{R_k} . That is,

$$\begin{aligned} \mathbf{v}_k &= f_k(\mathbf{x}_k; \theta_k) \in \mathbb{R}^{m_k}, \quad \forall k \in [1 : K], \\ \mathbf{z}_k &= \mathcal{Q}_k(\mathbf{v}_k), \quad \forall k \in [1 : K]. \end{aligned} \quad (15)$$

Given $\mathbf{z} = [\mathbf{z}_1, \mathbf{z}_2, \dots, \mathbf{z}_K]$ as input, the decoder \mathcal{D} first applies an initial mapping \mathcal{G} that takes \mathbf{z} to $\mathbb{R}^{\bar{m}}$, where $\bar{m} = \sum_{k=1}^K m_k$. This serves as a *combiner* for the values $\{\mathbf{z}_k\}_{k=1}^K$ received from the different encoders. Afterwards, a neural network $g(\cdot; \phi)$, parameterized by ϕ , is applied on the output of \mathcal{G} (see Figure 5) before feeding the output $\hat{\mathbf{x}}$ to the classifier \mathcal{C} . Thus, we have

$$\begin{aligned} \mathcal{G} &: \prod_{k=1}^K \mathcal{M}_k \rightarrow \mathbb{R}^{\bar{m}} \\ g(\cdot; \phi) &: \mathbb{R}^{\bar{m}} \rightarrow \mathcal{X}^n \\ \hat{\mathbf{x}} &= \mathcal{D}(\mathbf{z}) = g(\mathcal{G}(\mathbf{z}); \phi). \end{aligned} \quad (16)$$

Our objective is to minimize the misclassification loss

$$\min_{\theta_k, \mathcal{Q}_k, \mathcal{G}, \phi} \frac{1}{N} \sum_{i=1}^N [\mathbb{I}(\hat{y}(\hat{\mathbf{x}}^{(i)}) \neq y(\mathbf{x}^{(i)}))]. \quad (17)$$

Instead of minimizing the 0/1 loss function in (17), we construct a distribution from the output of the classifier \mathcal{C} using a softmax layer, and then apply the cross entropy loss to find the maximum likelihood estimator of $y(\mathbf{x})$ [44] using the samples in dataset \mathcal{T} . Hence, our objective is to minimize

$$\min_{\theta_k, \mathcal{Q}_k, \mathcal{G}, \phi} \mathcal{L}^c = \min_{\theta_k, \mathcal{Q}_k, \mathcal{G}, \phi} \frac{1}{N} \sum_{i=1}^N -\log(\text{softmax}[\mathcal{C}(\widehat{\mathbf{x}}^{(i)})]_{y(\mathbf{x}^{(i)})}), \quad (18)$$

where $[\text{softmax}(\mathbf{u})]_j = \exp(u_j) / \sum_{i=1}^{|\mathcal{Y}|} \exp(u_i)$.

We next discuss a challenge in applying standard backpropagation techniques for training our neural networks. Since the classifier \mathcal{C} is subdifferentiable, it is possible to compute the gradient of the cross entropy loss in (18) with respect to the decoder parameters ϕ . However, regardless of how the quantizers \mathcal{Q}_k are designed, the only subgradient of the quantizers is all zeros. As a result, it is not possible to apply backpropagation methods [5], [6], [45] to update the encoders parameters $\{\theta_k\}_{k=1}^K$. In the following two subsections, we introduce two different approaches for designing the quantizers $\{\mathcal{Q}_k\}_{k=1}^K$ and the combiner \mathcal{G} , and discuss how to incorporate their design in the learning framework of the neural network parameters $\{\theta_k\}_{k=1}^K$ and ϕ .

Remark 9. Note that we do not optimize the classifier \mathcal{C} as it is assumed to be pretrained and fixed. However, since the approaches discussed in this section are gradient-based, they can be directly extended to the case where the classifier \mathcal{C} is trainable as well, i.e., we can update the parameters of the classifier \mathcal{C} as we update the parameters of the networks f_k and g of the encoders and decoders.

A. Discrete distributed neural representation for classification:

In the first approach, we explicitly design the encoders to produce binary string representations of \mathbf{z}_k . In particular, for each encoder \mathcal{E}_k , the neural network $f_k(\cdot; \theta_k)$ outputs a vector with R_k entries ($m_k = R_k$), and we constrain the range of the elements of this vector to be in $[-1, 1]$. We achieve this by selecting the activations of the last layer of the neural network $f_k(\cdot; \theta_k)$ to be a function that has the range $[-1, 1]$ (we used the $\tanh(\cdot)$ function in our numerical evaluation). We then simply quantize the output values, by applying the quantizer \mathcal{Q}_k as

$$\mathcal{Q}_k(\mathbf{u}) = 2 * \mathbb{I}(\mathbf{u} \geq 0) - 1, \quad \forall k \in [1 : K], \quad (19)$$

where the indicator function \mathbb{I} is applied elementwise. For the combiner \mathcal{G} in the decoder we simply use an identity function.

Remark 10. As discussed above the \mathcal{Q}_k function prevents the backpropagation of the gradient to the encoder network $f_k(\cdot; \theta_k)$. To alleviate this, a straight-through approach is to only use the quantizer blocks in the forward pass and treat them as an identity during backpropagation [5], [45]. This approach works well in some applications [5], however, we observed in our experiments that such an approach prevented the encoder parameters $\{\theta_k\}_{k=1}^K$ from having meaningful gradient updates, and the end-to-end system had a classification performance close to random guessing in the CIFAR10 dataset. In particular, this can happen as when applying the chain rule during backpropagation, we would like to have the derivative $\partial\mathcal{L}^c/\partial\mathbf{v}_k$ to update the parameters θ_k , where $\mathbf{v}_k = f_k(\mathbf{x}_{\Omega_k}; \theta_k)$. Instead, the straight-through approach would use the gradient of a different point in space

$$\frac{\partial\mathcal{L}^c}{\partial\mathbf{z}_k} = \frac{\partial\mathcal{L}^c}{\partial(\mathbf{v}_k + (\mathbf{z}_k - \mathbf{v}_k))},$$

to update θ_k , where $\mathbf{z}_k = \mathcal{Q}_k(\mathbf{v}_k)$ (as in Figure 5). This can be very different from the intended gradient depending on how \mathcal{L}^c looks as a function of \mathbf{z}_k and how big is the second term $(\mathbf{z}_k - \mathbf{v}_k)$. As an illustration, if one choice of θ_k results in $v_k = 10^{-6}$ (very close to 0), it would get quantized to $\mathbf{z}_k = 1$, resulting in quantization noise $\mathbf{z}_k - \mathbf{v}_k = 1 - 10^{-6}$; if a different θ_k results in \mathbf{v}_k being very close to 1, it would again get quantized to 1, in this case with negligible quantization noise. Both parameters θ_k would be updated by the same gradient, even though in the first case, \mathbf{v}_k was orders of magnitude smaller. Thus, when skipping the quantizer in the backpropagation, the calculated gradients may not be useful if the quantization noise is large.

Regularization for quantization: Based on the observation in Remark 10, we opted to facilitate gradient-based optimization by dropping the quantizers blocks $\{\mathcal{Q}_k\}_{k=1}^K$ during training (both in the forward and backward passes) and instead nudge the network to naturally output values close to quantized ones. In particular, we penalize the output values that are far from both -1 and $+1$, by introducing an additional term to the loss in (18), termed *quantization loss*, and calculated as

$$\mathcal{L}^q = -\frac{1}{KN} \sum_{i=1}^N \sum_{k=1}^K \left\| f_k(\mathbf{x}_{\Omega_k}^{(i)}; \theta_k) \right\|_2^2. \quad (20)$$

Note that since we choose the activations of the last layer in each encoder to have the range $[-1, 1]$, \mathcal{L}^q is minimized (achieves the optimal value $-\sum_k R_k/K$) only when $f_k(\mathbf{x}_{\Omega_k}^{(i)}; \theta_k) \in$

$\{-1, 1\}^{R_k} \forall i \in [1 : N], k \in [1 : K]$. Thus, the total training loss becomes

$$\mathcal{L} = \mathcal{L}^c + \beta \mathcal{L}^q = -\frac{1}{N} \sum_{i=1}^N \left(\log (\text{softmax}[\widehat{y}(\widehat{\mathbf{x}}^{(i)})]_{y(\mathbf{x}^{(i)})}) - \beta \frac{1}{K} \sum_{k=1}^K \left\| f_k(\mathbf{x}_{\Omega_k}^{(i)}; \theta_k) \right\|_2^2 \right), \quad (21)$$

where: (i) β is a scalar hyperparameter that controls the contribution of \mathcal{L}^q ; and (ii) \mathcal{L}^c is the misclassification loss in (18).

For large enough β , minimizing \mathcal{L} can be interpreted as minimizing the classification loss under the constraint that the encoders outputs are very close to $-1/1$, which results in $\|f_k(\mathbf{x}_{\Omega_k}^{(i)}; \theta_k) - \mathcal{Q}_k(f_k(\mathbf{x}_{\Omega_k}^{(i)}; \theta_k))\|_2$ being very small. That is, the outputs without quantization differ by only a small amount from the outputs with quantization which can be treated as negligible quantization noise during testing.

To illustrate the impact of the *quantization loss* on the distribution of the encoder outputs, Figure 6 shows the empirical distribution of the encoders outputs after 50 training epochs on the CIFAR-10 dataset, with and without using \mathcal{L}^q . While the classification loss tries to direct the parameters of the encoders and decoder $\{\theta_k\}, \phi$ to improve the classification accuracy, the quantization loss adjusts the parameters to push the encoders outputs to be close to $-1/1$.

In the approach discussed in this subsection, we have integrated the quantization during the training phase by modifying the loss function to favor models that have small added noise due to quantization. Instead of modifying the objective function, in the following subsection, we introduce a multi-phase approach, where we first learn continuous representations for classification and then learn a quantizer on these continuous representations using our previously introduced GBI algorithm.

Remark 11. Note that the learning approach described in this subsection has computational complexity $O(N * \text{num_epochs})$, where `num_epochs` is typically much smaller than N .

B. Distributed neural representation using GBI:

The main idea in this approach is to use the GBI algorithm to design the quantizers $\{\mathcal{Q}_k\}_{k=1}^K$ and the initial decoder \mathcal{G} . We first use the neural network $f_k(\cdot; \theta_k)$ to map the features of node k from $\mathbf{x}_{\Omega_k} \in \mathbb{R}^{|\Omega_k|}$ to $\mathbf{v}_k \in \mathbb{R}^{m_k}$. We select m_k to be as small as possible while maintaining a good classification accuracy; that is, the networks $f_k(\cdot; \theta_k)$ essentially perform dimensionality reduction at the encoders before applying the quantization step. We then apply GBI on the output of the encoder neural network f_k . The main benefit is that, by decreasing the number of

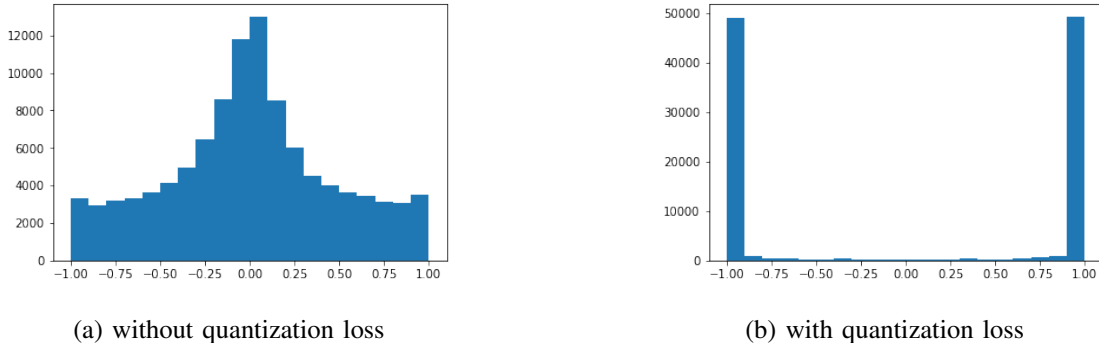


Fig. 6: Effect of the quantization loss on the distribution of the decoder inputs after training for 50 epochs on the CIFAR10 dataset.

dimensions of the input to GBI algorithm, we alleviate the complexity of GBI, that grows with the number of dimensions (see Section V).

Given that the neural network $f_k(\cdot; \theta_k)$ is potentially a universal function approximator [46], it is not difficult to see that even using a naive uniform quantizer \mathcal{Q}_k , we could potentially implement any encoder $\mathcal{E}_k = \mathcal{Q}_k(f_k(\cdot; \theta_k)) : \mathbb{R}^{|\Omega_k|} \rightarrow \mathcal{M}_k$. Hence, ideally, the choice of the quantizer \mathcal{Q}_k should not play a significant role. However, due to the fact that neural networks tend to work well only if the initialization is close to a good solution, the choice of the quantizer becomes important. In the following, we propose a method that operates in three phases:

Phase 1. We first train the encoders and decoder neural networks without any quantization units (i.e., without \mathcal{Q}_k and \mathcal{G}) until we get classification accuracy that is close to the classifier’s accuracy. Note that for $m_k \geq |\Omega_k|$, we can reconstruct the classifier accuracy. Effectively, in this step, we are following the example structure shown in Figure 5, assuming the blocks \mathcal{Q}_k and \mathcal{G} are identities.

Phase 2. With the parameters θ_k, ϕ learned in **Phase 1**, we now design the quantization components $\{\mathcal{Q}_k\}_{k=1}^K$ and \mathcal{G} based on the outputs $\{\mathbf{v}_k\}$ of the neural networks $f_k(\cdot; \theta_k)$. If the quantizer maps data points that have different labels to the same quantized value, the quantized value cannot be used to classify the points correctly. Hence, the objective of the quantizer is to map points that have different labels to different quantized values. We do this by introducing boundaries in the space using our proposed GBI quantizer, described earlier in Section V.

Phase 3. Finally, we continue training the encoders and decoder neural networks (f_k and g) with the quantizers designed in **Phase 2**. To do so we skip the quantizers blocks in the back

propagation and consider them only in the forward pass. We observed in our experiments that this skip does not cause the network to behave randomly as the initialization is designed carefully. The parameters learned in **Phase 1** act as initializations for θ_k, ϕ in this phase. Phase 3 enables to fine tune the network parameters given that we have already learned the quantizer components earlier in **Phase 2**.

VII. EXPERIMENTAL EVALUATION

In this section, we present various experimental results, comparing the behaviour of our proposed distributed quantization approaches with quantization approaches for reconstruction. We find that tailoring the quantizers to the classification task can offer significant savings: we can achieve more than a factor of two reduction in terms of the number of bits communicated, for the same classification accuracy. Moreover, our algorithms retain reasonable classification performance even when constrained to use a very small number of bits per encoder; for instance, for 2 bits per encoder, we achieve approximately two to four times the classification accuracy of alternative approaches.

Additionally, we also compare to centralized quantization approaches for classification and show that despite our distributed setup, we are still able to achieve a competitive performance in terms of classification accuracy.

A. Performance on Electromyography sensor measurements:

We start with experiments on a dataset of surface electromyographic (sEMG) signals [47]. Each data point represents measurements recorded from 8 sensors that are used to differentiate between 6 different hand gestures. For our classifier \mathcal{C} , we use a Multi-Layer Perceptron (MLP) [44] architecture with fully connected layers of the form $8 - 100 - 200 - 200 - 200 - 6$ and ReLU activations. The classifier was pretrained on an unquantized training set of 15,345 measurements, and yielded a baseline accuracy of 98.66% on a test set of 6,578 measurements.

For our distributed quantization framework, we assume that we have $K = 4$ encoders, where each encoder has access to measurements from only two of the sensors (i.e., we have four feature groups each consisting of two features). We use MLPs for our encoders and decoder, while the quantizers are either trained using the quantization loss regularization (**NN-REG**) or with the GBI algorithm (**NN-GBI**) as described in Section VI. The hidden layers structures

	bits per encoder (R)				
	1	2	3	4	5
<i>k</i> -means [48]	18.77%	44.18%	56.47%	66.71%	75.19%
NN-REG	54.50%	63.04%	82.90%	94.72%	97.73%
NN-GBI	55.49%	72.35%	91.12%	97.30%	98.21%

TABLE II: Correct classification percentage on the sEMG test set. Each system uses R bits per encoder, $K = 4$ encoders and a pretrained classifier with 98.66% accuracy.

of encoders/decoders, and the hyper parameters (learning rate and regularization weight β) are described in Appendix E.

Comparison with quantization for reconstruction. We demonstrate that our approaches achieve competitive classification results with smaller number of bits as compared to distributed approaches aiming at reconstructing the input. We compare against the k -means algorithm [48] as a representative for unsupervised vector quantization algorithms. In particular, in the sEMG dataset, each k -means encoder maps a point in \mathbb{R}^2 to the nearest centroid point among 2^R choices. The decoder is treated as an identity in this case, that passes its input \mathbf{z} vector to the classifier.

The results are shown in Table II. We see that our approaches outperform the unsupervised distributed quantization. For example, using 4 bits for each encoder, we can achieve a classification accuracy of $> 95\%$ while the unsupervised approach achieves a performance of 66%.

Comparison with learning vector quantization for classification. To benchmark the performance of our distributed quantization system for classification against centralized approaches, a natural candidate for comparison is the centralized Generalized Learning Vector Quantization approach (GLVQ) [22]. In this case, the output of the algorithm is a Voronoi tessellation in the space, where each centroid is now associated with a class. Thus, by mapping a point in space to its nearest centroid, a classification is also performed by picking the class associated to the selected centroid. We compare the performance of our distributed quantization approaches against the quantizer-classifier learned by the LVQ3 centralized quantizer [22] with learning rate 10^{-4} for 200 epochs.

Since our distributed quantization system with $K = 4$ encoders uses 2 bits per encoder, we allow LVQ3 to use 8 bits (i.e., 64 centroids) to keep the total number of bits across the nodes constant. Our **NN-GBI** approach, yielded 71.59% classification accuracy, while the centralized

LVQ classifier gave an accuracy of 75.53%.

Although LVQ gives a better classification accuracy, the learned Voronoi boundaries are not decomposable to be applied on distributed nodes. In particular, in the described setting, when inspecting the values of the centroids learned by the LVQ algorithm, we found that although 2^8 centroids are used in \mathbb{R}^8 , restricting the values of the centroids to any one dimension of the 8, gave 64 distinct values which would require each of the 4 encoders to at least use 8 bits to represent these quantized values. Recall that from Table II, we are able to achieve much higher accuracies than 75%, when only 5 bits are used at each encoder.

B. Performance on CIFAR10 images:

In this set of experiments, we evaluate the performance of our proposed algorithms on the CIFAR10 dataset, where each input \mathbf{x} is a $32 \times 32 \times 3$ image. Each image in the CIFAR10 dataset is associated with one of 10 classes. We assume a distributed quantization system with $K = 4$ distributed encoders, that each have access to a quadrant of the image. For the classifier, we use a pretrained VGG-13 classifier [49] with 94.27% accuracy on the CIFAR10 test dataset.

Comparison to VQ-VAE. The VQ-VAE [5] framework is used to learn discrete neural representations of a dataset for reconstruction. We compare against this framework implemented both in a centralized and a distributed fashion. In particular, for the centralized VQ-VAE, a single encoder has access to the full image. We use the same VQ-VAE network structure from [5] for the CIFAR10 dataset and ensure that the total number of bits used by the VQ-VAE encoder is 4 times what our system would use for a single encoder. In the distributed setting, a VQ-VAE encoder is applied on each image quadrant and then a common decoder is used for reconstruction. VQ-VAE structures were trained with 2×10^{-4} learning rate, 200 epochs and 64 batch size.

The results are summarized in Table III. We find that although VQ-VAE has shown great success in reconstructing images from discrete representations, it does not perform well with a low number of bits even in the centralized case. To get classification accuracy of around 50%, the centralized VQ-VAE required 200 bits (equivalent to 50 bits/encoder in the distributed setting), while our algorithms could get more than 70% accuracy with 3 bits per encoder.

VIII. CONCLUSIONS

In this paper, we introduced the problem of data-driven distributed data quantization for classification. We proved that in many cases, designing an optimal quantization system is an

	bits per encoder (R)				
	1	2	3	4	5
VQ-VAE (centralized)	13.82%	14.36%	15.87%	17.52%	18.18%
VQ-VAE (distributed)	10.12%	10.46%	11.03%	11.61%	12.28%
NN-REG	48.63%	63.32%	68.07%	73.43%	78.12%
NN-GBI	48.33%	60.88%	65.16%	71.57%	81.18%

TABLE III: Correct classification percentage on the CIFAR10 test set. All distributed systems use R bits per encoder, $K = 4$ encoders. The centralized VQ-VAE system uses $4R$ bits at the encoder. The classifier is a pretrained VGG-13 with 94.27% accuracy.

NP-hard problem that is also hard to approximate. For a case that is not NP-hard, we proposed an optimal polynomial-time algorithm for designing the quantizer under some structural restrictions. For the NP-hard cases, we proposed a polynomial time greedy approach and two learning based approaches. Numerical results on the sEMG and CIFAR10 datasets indicate that tailoring the quantizers to the classification task can offer significant savings: more (and in some cases much more) than a factor of two reduction in the number of bits communicated, for the same classification accuracy. Moreover, our algorithms retain reasonable classification performance even when constrained to use a very small number of bits.

APPENDIX A

COUNTER-EXAMPLE FOR ADABOOST INSPIRED QUANTIZATION

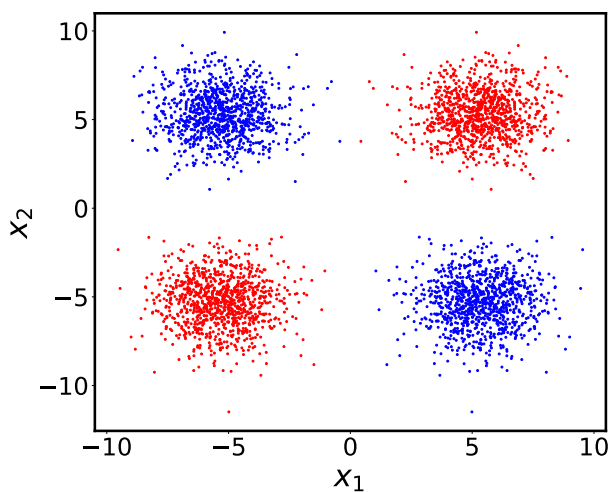


Fig. 7: Xor-like example where Adaboost inspired quantization would fail.

APPENDIX B

NP-HARDNESS AND HARDNESS OF APPROXIMATION

In this appendix we prove Theorem 1.

A. NP-hardness of **(P1')** and **(P2')**

In this subsection, we prove that **(P1')**, **(P2')** are NP-hard. We start with **(P2')**. Since **(P2')** is a special case of **(P1')**; it follows that **(P1')** is NP-hard. We prove hardness of **(P2')** by reduction from the Chromatic Number problem. In particular, we show that any instance of the Chromatic Number problem can be reduced to an instance of problem **(P2')** in polynomial time. The decision version of the Chromatic Number problem is on Karp's list of NP-complete problems [50].

Let us consider an undirected graph G . We denote the set of vertices and edges of G by V, E respectively, and assume that the vertices are labeled by numbers $1, 2, \dots, |V|$. Since the graph is undirected, we assume without loss of generality that the vertices pair corresponding to each edge is ordered such that if $(q_1, q_2) \in E$, then $q_1 > q_2$. We will see that this assumption, ensures that we can construct a linearly separable dataset as required in problem **(P2')**.

We construct two matrices $\{F_i\}_{i=0}^1, F_i \in \mathbb{R}^{|E| \times |V|}$ that represent the set of edges E , by Algorithm 3. We can think of the matrices $\{F_i\}_{i=0}^1$ as a decomposed version of the incidence matrix,

Algorithm 3 Incidence matrices

0: Initialize the entries of $F_i \in \mathbb{R}^{|E| \times |V|}, i \in \{0, 1\}$ with all zeros. $k = 1$.

$\forall (q_1, q_2) \in E$, do the following two steps:

1: Put $[F_0]_{kq_1} = 1, [F_1]_{kq_2} = 1$.

2: $k=k+1$.

where for each edge, one endpoint is represented in F_0 and the other endpoint is represented in F_1 . As an illustrative example, we consider the graph in Figure 8. The corresponding matrices are given by

$$F_0 = \begin{bmatrix} 0 & 0 & 1 & 0 & 0 \\ 0 & 0 & 0 & 1 & 0 \\ 0 & 0 & 0 & 0 & 1 \\ 0 & 0 & 0 & 1 & 0 \\ 0 & 0 & 0 & 1 & 0 \\ 0 & 0 & 0 & 0 & 1 \\ 0 & 0 & 0 & 0 & 1 \\ 0 & 1 & 0 & 0 & 0 \end{bmatrix}, F_1 = \begin{bmatrix} 1 & 0 & 0 & 0 & 0 \\ 1 & 0 & 0 & 0 & 0 \\ 1 & 0 & 0 & 0 & 0 \\ 0 & 1 & 0 & 0 & 0 \\ 0 & 0 & 1 & 0 & 0 \\ 0 & 0 & 1 & 0 & 0 \\ 0 & 0 & 0 & 1 & 0 \\ 1 & 0 & 0 & 0 & 0 \end{bmatrix}. \quad (22)$$

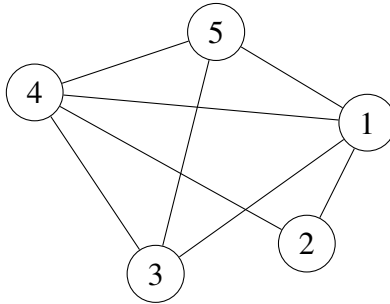


Fig. 8: Graph with edges represented by the matrices in (22).

If two vertices are colored with the same color, we update the matrices $\{F_i\}_{i=0}^1$ by replacing the columns that correspond to the vertices colored with the same color, with their sum. For example, if vertices 1, 2 are assigned the same color, we update each matrix F_i by replacing the first two columns with their sum, which results in

$$F'_0 = \begin{bmatrix} 0 & 1 & 0 & 0 \\ 0 & 0 & 1 & 0 \\ 0 & 0 & 0 & 1 \\ 0 & 0 & 1 & 0 \\ 0 & 0 & 1 & 0 \\ 0 & 0 & 0 & 1 \\ 0 & 0 & 0 & 1 \\ 1 & 0 & 0 & 0 \end{bmatrix}, F'_1 = \begin{bmatrix} 1 & 0 & 0 & 0 \\ 1 & 0 & 0 & 0 \\ 1 & 0 & 0 & 0 \\ 1 & 0 & 0 & 0 \\ 0 & 1 & 0 & 0 \\ 0 & 1 & 0 & 0 \\ 0 & 0 & 1 & 0 \\ 1 & 0 & 0 & 0 \end{bmatrix}. \quad (23)$$

We notice that **a coloring is valid** (no two vertices connected with an edge are assigned the same color) if and only if the updated matrices satisfy:

$$\forall k \in [1 : |E|], \forall q \in [1 : V'], \forall i \in \{0, 1\} \quad : \quad [F'_i]_{kq} \neq 0 \implies [F'_{1-i}]_{kq} = 0, \quad (24)$$

where V' is the number of columns of the matrix F'_0 or F'_1 . In the above example, the property in (24) is not satisfied since, $[F'_i]_{80} = 1, [F'_{1-i}]_{81} = 1$. This is because the vertices 1, 2, which are assigned the same color, are connected with an edge.

Hence, the Chromatic Number of the graph is the minimum number of columns of matrices $\{F'_i\}_{i=0}^1$ that satisfy the property in (24) and are constructed according to the following rules:

- Any set of columns in the matrix F'_i can be replaced by their sum, $i = 0, 1$.
- If the set of columns indexed by \mathcal{I} in F'_i are replaced with their sum, then the set of columns indexed by \mathcal{I} in F'_{1-i} are replaced with their sum, $i = 0, 1$, i.e., exactly the same operations done on F'_0 are done on F'_1 and vice versa.

The next step is to consider an instance from the problem **(P2')**, and show that it is equivalent to the problem of finding the minimum number of columns of the matrices $\{F'_i\}_{i=0}^1$. To that end, we consider a dataset, with two classes, namely $\mathcal{Y} = \{0, 1\}$, and two features x_1, x_2 . The dataset is constructed based on the matrices $\{F'_i\}_{i=0}^1$ by Algorithm 4.

Algorithm 4 Reduction from vertex coloring problem

0: Start with $k = 1$.

$\forall (q_1, q_2) \in E$, do the following two steps:

1: Put a training point that belong to class 0 at $x_1 = q_1, x_2 = \frac{q_1+q_2}{2}$,

and a training point that belong to class 1 at $x_1 = q_2, x_2 = \frac{q_1+q_2}{2}$.

2: $k=k+1$.

Note that under the assumption $q_1 > q_2$, the point $(x_1, x_2) = (q_1, \frac{q_1+q_2}{2})$ lies on the right side of the line $x_1 = x_2$, while the point $(x_1, x_2) = (q_2, \frac{q_1+q_2}{2})$ lies on the left side of the line $x_1 = x_2$. Hence, all the points that belong to class 0 lie on the right side of the line $x_1 = x_2$, and all the points that belong to class 1 lie on the left side of the line $x_1 = x_2$. That is, the constructed dataset is linearly separable by the line $x_1 = x_2$.

For the constructed dataset, we want to answer the following question: for $R_2 \rightarrow \infty$, what is the minimum R_1 for which $\mathcal{L}(\mathcal{E}, \mathcal{D}, \mathcal{T}) < \frac{1}{2}$?

As an example, consider the matrices $\{F_i\}_{i=0}^1$ in (22), the constructed dataset is given in Figure 9.

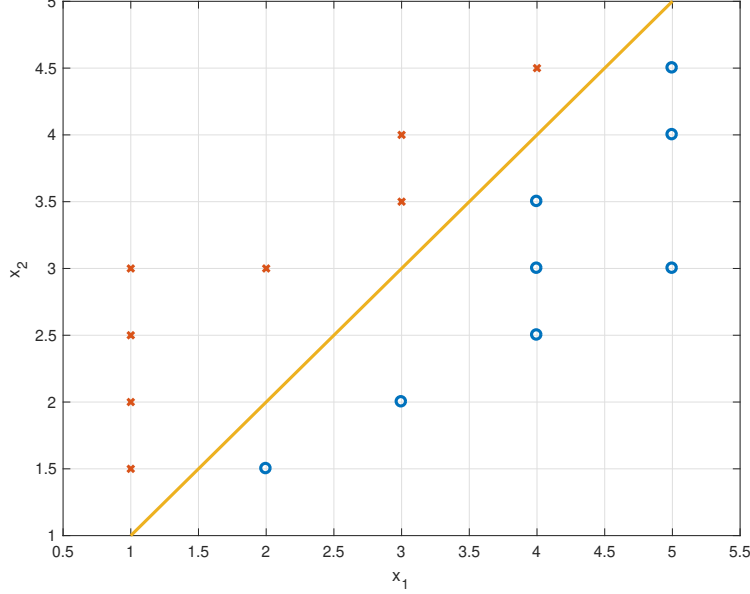


Fig. 9: Training data corresponding to $\{F_i\}$ in (22).

Assume that we want to find the minimum R_1 for which $\mathcal{L}(\mathcal{E}, \mathcal{D}, \mathcal{T}) < \frac{1}{2}$. If $2^{R_1} \geq 5$, then we do not need to do quantization and can send x_1 as it is. In this case we have $\mathcal{L}(\mathcal{E}, \mathcal{D}, \mathcal{T}) = 0$. Now, assume that $2^{R_1} = 4$, then we have only 4 values to send to represent x_1 , i.e., $\mathcal{E}_1(x_1) \in [1 : 4]$. Hence, the quantizer has to map two different values of x_1 to the same quantized value, i.e., $\exists x_1^{(1)}, x_1^{(2)} : x_1^{(1)} \neq x_1^{(2)}, \mathcal{E}_1(x_1^{(1)}) = \mathcal{E}_1(x_1^{(2)})$. The matrices $\{F'_i\}$ are constructed from $\{F_i\}$ such that if the encoder maps a set of x_1 values to the same encoded value, we replace the corresponding columns with their sum. For instance, assume that the encoder maps the values $x_1 = 1, x_1 = 2$ to the same quantized value. Based on this, we update each matrix F_i by replacing the first two columns with their sum, which results in the matrices in (23). Since this encoder maps the two points $(1, 1.5), (2, 1.5)$, which belong to different classes, to the same encoded value, we have $\mathcal{L}(\mathcal{E}, \mathcal{D}, \mathcal{T}) = \sum_{k=1}^{l_2} \sum_{q=1}^{l_1-1} \min_j \{[F'_j]_{kq}\} = 1 > \frac{1}{2}$. So, this encoder does not satisfy $\mathcal{L}(\mathcal{E}, \mathcal{D}, \mathcal{T}) < \frac{1}{2}$. The reason for this is that the updated matrices do not satisfy: $\forall k \in [1 : |E|] \forall q \in [1 : |V'|] \forall i \in \{0, 1\} [F'_i]_{kq} \neq 0 \implies [F'_{1-i}]_{kq} = 0$. Note that the matrices constructed by Algorithm 3 satisfy the following properties

- Every row in F'_i has exactly one non-zero entry.

- If $[F_i]_{kq} \neq 0$, then $[F_{1-i}]_{kq} = 0$.
- All the non-zero entries have value 1.

It is easy to observe that for all matrices satisfying the three properties mentioned above, $\mathcal{L}(\mathcal{E}, \mathcal{D}, \mathcal{T}) < \frac{1}{2}$ if and only if the encoder \mathcal{E} satisfies:

$$\begin{aligned} & \forall q_1 \forall q_2 : q_1, q_2 \in \text{dom}(\mathcal{E}_1), q_1 \neq q_2, \mathcal{E}_1(q_1) = \mathcal{E}_1(q_2) \\ & [\forall k \in [1 : |E|] \forall i \in \{0, 1\} ([F_i]_{kq_1} + [F_i]_{kq_2} \neq 0 \implies [F_{1-i}]_{kq_1} + [F_{1-i}]_{kq_2} = 0)]. \end{aligned} \quad (25)$$

Hence, the $\min\{2^{R_1} | \mathcal{L}(\mathcal{E}, \mathcal{D}, \mathcal{T}) < \frac{1}{2}\}$ is the minimum number of columns of matrices $\{F'_i\}_{i=0}^1$ that satisfy the property in (24) and are constructed according to the following rules:

- Any set of columns in the matrix F_i can be replaced by their sum, $i = 0, 1$.
- If the set of columns indexed by \mathcal{I} in F_i are replaced with their sum, then the set of columns indexed by \mathcal{I} in F_{1-i} are replaced with their sum, $i = 0, 1$, i.e., exactly the same operations done on F_0 are done on F_1 and vice versa.

This shows that $\mathcal{X}(G) = \min\{2^{R_1} | \mathcal{L}(\mathcal{E}, \mathcal{D}, \mathcal{T}_G) < \frac{1}{2}\}$, where $\mathcal{X}(G)$ is the chromatic number of the graph G , and \mathcal{T}_G is the dataset constructed by Algorithm 4.

Note that the maximum number of x_1 values that are encoded to the same value is $|V|$, i.e., $\mathcal{E}_1(\mathbf{z}_1)$ is the union of at most $|V|$ \mathbb{R} -bins. Hence, r is chosen to be $r = |V|$. This concludes the proof that problem **(P2')** is NP-hard.

B. NP-hardness of **(P3')**:

In this subsection, we prove that **(P3')** is NP-hard. For reference, we restate the statement of **(P3')** below:

(P3') : For $n = 2$ features, $|\mathcal{Y}| = 2$ classes, find the minimum $R_1 = R_2$ bits for which $\mathcal{L}(\mathcal{E}, \mathcal{D}, \mathcal{T}) < p_e$, assuming that $\mathcal{E}_k^{-1}(\mathbf{z}_k)$ is a single \mathcal{X}_{Ω_k} -bin.

To prove that **(P3')** is NP-hard, we show that the maximum Balanced Complete Bipartite Subgraph (BCBS) problem [51] can be reduced to **(P3')** in polynomial-time. The maximum BCBS problem is defined below.

Definition 2. (*maximum BCBS*) Given a balanced bipartite graph $G = (V_1, V_2, E)$: find the maximum size, in terms of number of vertices, of a balanced bi-clique in G^6 .

⁶By a balanced bipartite graph G , we mean that $|V_1| = |V_2|$.

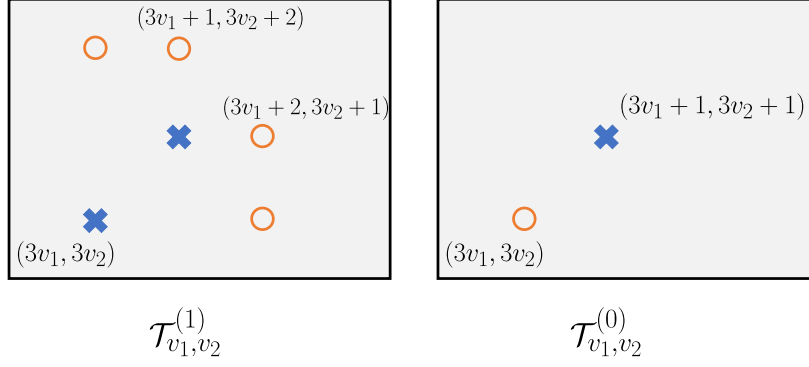


Fig. 10: Structures of gadget datasets $T_{v_1, v_2}^{(1)}$ and $T_{v_1, v_2}^{(0)}$.

The maximum BCBS problem is known to be NP-hard as proved in [51].

We start by considering the case where the minimum degree in G is nonzero and then address the case, where there are vertices with zero degree afterwards.

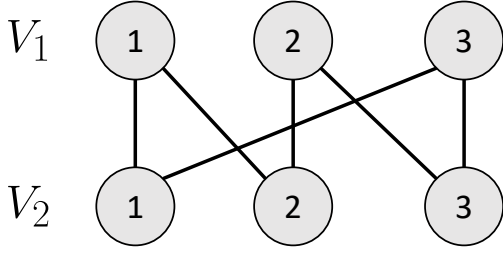
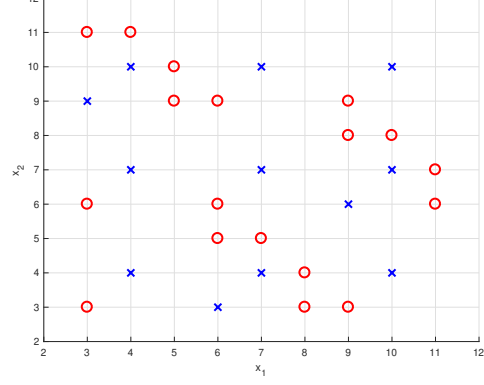
Our first step in the reduction is to construct a dataset $\mathcal{T}_G = \{(\mathbf{x}, y(\mathbf{x}))\}$ based on the graph G . To do so, we model each pair of vertices $(v_1, v_2) \in [1 : V_1(G)] \times [1 : V_2(G)]$ as a gadget dataset \mathcal{T}_{v_1, v_2} of labeled points $(\mathbf{x}, y(\mathbf{x}))$, where v_1, v_2 are the indices of the vertex pair. The dataset \mathcal{T}_{v_1, v_2} can take one of two choices ($\mathcal{T}_{v_1, v_2}^{(1)}$ or $\mathcal{T}_{v_1, v_2}^{(0)}$) depending on whether $(v_1, v_2) \in E$ or not, respectively. In particular, these two gadget choices are defined below

$$\begin{aligned} \mathcal{T}_{v_1, v_2}^{(1)} = \{ & ([3v_1, 3v_2], 1), ([3v_1+1, 3v_2+1], 1), \\ & ([3v_1+2, 3v_2], 0), ([3v_1+2, 3v_2+1], 0), \\ & ([3v_1, 3v_2+2], 0), ([3v_1+1, 3v_2+2], 0)\} \quad \text{if } (v_1, v_2) \in E, \end{aligned} \quad (26)$$

$$\mathcal{T}_{v_1, v_2}^{(0)} = \{([3v_1, 3v_2], 0), ([3v_1+1, 3v_2+1], 1)\} \quad \text{if } (v_1, v_2) \notin E. \quad (27)$$

Figure 10 shows an illustration of the two possible versions of \mathcal{T}_{v_1, v_2} . The constructed dataset \mathcal{T}_G is the union of all gadget dataset \mathcal{T}_{v_1, v_2} , $\forall v_1, v_2$, i.e.,

$$\mathcal{T}_G = \bigcup_{(v_1, v_2) \in [1:V_1(G)] \times [1:V_2(G)]} \mathcal{T}_{v_1, v_2}.$$

(a) Example graph G .(b) Dataset \mathcal{T}_G constructed from G .Fig. 11: Example of reduction from balanced bipartite graph G to dataset \mathcal{T}_G .

Example. Consider the example balanced bipartite graph $G = (V_1, V_2, E)$ shown in Figure 11a, where $|V_1| = |V_2| = 3$ and $E = \{(1, 1), (1, 2), (2, 2), (2, 3), (3, 1), (3, 3)\}$. The constructed dataset \mathcal{T}_G using the construction defined above is shown in Figure 11b.

Now, we would like to show that in the constructed dataset \mathcal{T}_G : finding the minimum $R_1 = R_2$ such that the $\mathcal{L}(\mathcal{E}, \mathcal{D}, \mathcal{T}_G) = 0$ is equivalent to finding the size of the maximum BCBS in G .

To do so, we first discuss the following properties of the gadget datasets $\mathcal{T}_{v_1, v_2}^{(1)}$ and $\mathcal{T}_{v_1, v_2}^{(2)}$ and the dataset \mathcal{T}_G below.

Properties of \mathcal{T}_G , $\mathcal{T}_{v_1, v_2}^{(1)}$ and $\mathcal{T}_{v_1, v_2}^{(2)}$.

- 1) Points in the dataset \mathcal{T}_G are arranged in **rows** and **columns** in \mathbb{R}^2 indexed by

$$\text{rows} = \bigcup_{v_2 \in [1:|V_2|]} \{3v_2, 3v_2 + 1, 3v_2 + 2\}, \quad \text{cols} = \bigcup_{v_1 \in [1:|V_1|]} \{3v_1, 3v_1 + 1, 3v_1 + 2\}$$

- 2) Since **(P3')** assumes $\mathcal{E}_k^{-1}(\mathbf{z}_k)$ is a single \mathcal{X}_{Ω_k} -bin, then quantization of x_1 (resp., x_2) in \mathcal{T}_G is equivalent to combining adjacent columns (resp., rows) in \mathcal{T}_G . Combining non-adjacent columns (resp., rows) is not allowed as it will not result in a single bin as assumed by **(P3')**. We say that two columns (resp., rows) are **combined**, if they are assigned to the same \mathbf{z}_1 (resp., \mathbf{z}_2);
- 3) For any $v_2 \in [1 : |V_2|]$, there exists a v_1 such that $\mathcal{T}_{v_1, v_2} = \mathcal{T}_{v_1, v_2}^{(1)}$, i.e., is of type 1. This is due to the fact that the vertex indexed by v_2 has a non-zero degree. A similar property exists, flipping the roles of v_1 and v_2 in the statement above;

- 4) Observing the structure of the gadget dataset $\mathcal{T}_{v_1, v_2}^{(1)}$ and $\mathcal{T}_{v_1, v_2}^{(0)}$ in Figure 10, it is not difficult to see that only the columns (resp., rows) corresponding to indices $x_1 = 3v_1, 3v_1 + 1$ (resp., $x_2 = 3v_2, 3v_2 + 1$) can be combined while maintaining $\mathcal{L}(\mathcal{E}, \mathcal{D}, \mathcal{T}_{v_1, v_2}) = 0$. For shorthand, we refer to action of combining these columns (resp., rows) with \mathbf{q}_{v_1} (resp., \mathbf{q}_{v_2}), where

$$\begin{aligned} \mathbf{q}_{v_1}: & \text{ combining the columns } x_1 = 3v_1, x_1 = 3v_1 + 1, \\ \mathbf{q}_{v_2}: & \text{ combining the rows } x_2 = 3v_2, x_2 = 3v_2 + 1. \end{aligned} \quad (28)$$

- 5) The dataset types $\mathcal{T}_{v_1, v_2}^{(1)}$ and $\mathcal{T}_{v_1, v_2}^{(0)}$ impose allowance and restriction relations on the possible quantizations (combining of columns/rows). It is not hard to see from Figure 10 that in $\mathcal{T}_{v_1, v_2}^{(1)}$, we can apply both combining actions \mathbf{q}_{v_1} and \mathbf{q}_{v_2} simultaneously without incurring any penalty in the misclassification loss. On the other hand, in $\mathcal{T}_{v_1, v_2}^{(0)}$, we cannot apply both combining actions \mathbf{q}_{v_1} and \mathbf{q}_{v_2} without incurring a misclassification loss (two points from different class will collapse to the same position and become indistinguishable after quantization). Thus we have the following equivalent relations in G and \mathcal{T}_G [**This is the key property in the reduction**]

$$(v_1, v_2) \notin E \iff \mathcal{T}_{v_1, v_2}^{(0)} \subseteq \mathcal{T}_G \iff \mathbf{q}_{v_1}, \mathbf{q}_{v_2} \text{ are mutually exclusive,} \quad (29)$$

and similarly

$$(v_1, v_2) \in E \iff \mathcal{T}_{v_1, v_2}^{(1)} \subseteq \mathcal{T}_G \iff \mathbf{q}_{v_1}, \mathbf{q}_{v_2} \text{ are not mutually exclusive.} \quad (30)$$

- 6) Property 3 and 4 together imply that in \mathcal{T}_G , columns (resp., rows) from different \mathcal{T}_{v_1, v_2} cannot be combined together while maintaining $\mathcal{L}(\mathcal{E}, \mathcal{D}, \mathcal{T}_{v_1, v_2}) = 0$. In other words, the only available quantization design actions that maintain zero loss are those defined by \mathbf{q}_{v_1} and \mathbf{q}_{v_2} in (28);
- 7) From Property 3, we have that the total number of columns (resp., rows) in the \mathcal{T}_G is equal to $3|V_1|$ (resp., $3|V_2|$).
- 8) From Property 7, by default, we would need $2^{R_1} = 3|V_1|$ and $2^{R_2} = 3|V_2| = 3|V_1|$ to represent the data without quantization (recall that $|V_1| = |V_2|$ as G is balanced).

With the previously observed properties, we can now state the equivalence between finding maximum BCBS and finding the minimum $R = R_1 = R_2$ that achieves $\mathcal{L}(\mathcal{E}, \mathcal{D}, \mathcal{T}_G) = 0$. In particular, we have that

Claim 1. Any quantization (combining) approach in \mathcal{T}_G with $2^R = 3|V_1| - W$ quantization bins for both x_1 and x_2 such that $\mathcal{L}(\mathcal{E}, \mathcal{D}, \mathcal{T}_{v_1, v_2}) = 0$ results in a BCBS in G of size W and vice versa.

By this relation between the number of bits R and the size of bi-clique W , we have that finding the maximum BCBS size in G is equivalent to finding the minimum R bits that results in $\mathcal{L}(\mathcal{E}, \mathcal{D}, \mathcal{T}_{v_1, v_2}) = 0$.

What remains is to prove both directions in Claim 1.

BCBS \rightarrow quantization: Assume that the maximum BCBS is equal to W . Then there exists a set $W_1 \subseteq [1 : |V_1|]$ and $W_2 \subseteq [1 : |V_1|]$ such that: (i) $|W_1| = |W_2| = W$; (ii) $\forall (w_1, w_2) \in W_1 \times W_2$, we have that $(w_1, w_2) \in E$ and $\mathcal{T}_{w_1, w_2}^{(1)} \subseteq \mathcal{T}_G$. As a result, we can apply the combining actions $\mathbf{q}_{w_1} \forall w_1 \in W_1$ and $\mathbf{q}_{w_2} \forall w_2 \in W_2$ while still maintaining zero loss as none of them are in conflict with one another (recall (1)). Thus, after applying these combinations, we are left with $3|V_1| - W$ columns and rows, which is our intended value for 2^R .

quantization \rightarrow BCBS: Assume that we have a zero loss quantization that uses $2^R = 3|V_1| - W$ bins for either x_1 and x_2 . Since, the possible combining actions are those given by (28), then there exists a set $W_1, W_2 \subseteq [1 : |V_1|]$, such that the given quantization is designed by applying \mathbf{q}_{w_1} and $\mathbf{q}_{w_2} \forall w_1 \in W_1, w_2 \in W_2$. Since, applying the aforementioned combining actions did not result in an increase in the loss, then by Property 4, we have that

$$\forall (w_1, w_2) \in W_1, W_2, (w_1, w_2) \in E.$$

Thus, we have that W_1 and W_2 index vertices in G that form a balanced bi-clique of size W .

This concludes the proof for the case, where all vertices in G have a non-zero degree.

Finally, let us assume that our bipartite graph G has some vertices with zero degrees. In particular let $G = G' \cup \widehat{G}$, where $G' = (V'_1, V'_2, E)$ is the subgraph with all vertices with non-zero degrees and $\widehat{G} = (\widehat{V}_1, \widehat{V}_2, \phi)$ be the bipartite graph combining all vertices with zero degrees.

Here, we can follow the same logic for G' to construct $\mathcal{T}_{G'}$. In addition, for \widehat{G} , we can add an additional dataset $\mathcal{T}_{\widehat{G}}$ (shown in Figure 12) such that $\mathcal{T}_{\widehat{G}}$ is a grid of points of size $3|\widehat{V}_1| \times 3|\widehat{V}_2|$ that cannot be quantized further with zero loss. $\mathcal{T}_G = \mathcal{T}_{G'} \cup \mathcal{T}_{\widehat{G}}$ as seen in Figure 12.

It is not difficult to see that Claim 1 extends to this case as well. This concludes the proof of NP-hardness of **(P3')**.

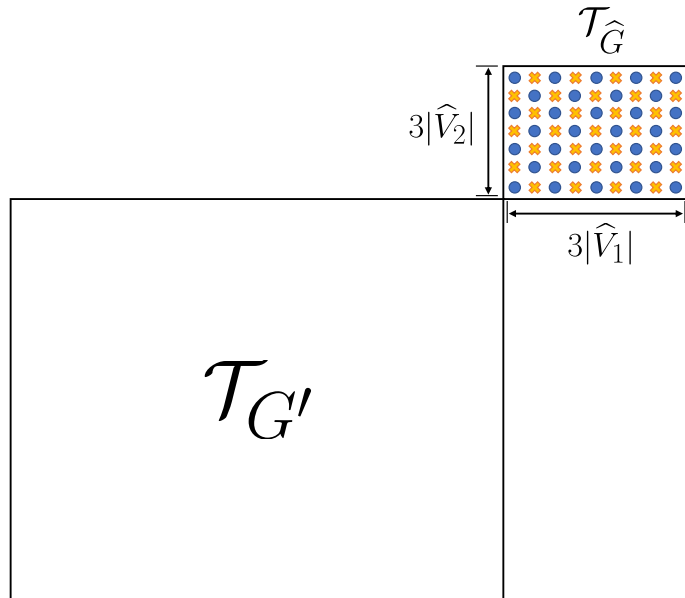


Fig. 12: Illustration of \mathcal{T}_G decomposition into $\mathcal{T}_{\hat{G}}$ and $\mathcal{T}_{G'}$.

C. NP-hardness of $(\mathbf{P4}')$

To prove $(\mathbf{P4}')$, we notice the following. Consider a training dataset with $n = 3$ features, where the training data points have arbitrary values for features x_1, x_2 , while feature x_3 takes values $x_3 = -1$ for all points that belong to class 0 and $x_3 = 1$ for all points that belong to class 1. Such training data points are linearly separable by the hyperplane $x_3 = 0$. However, if $R_3 = 0$, we cannot send any information based on feature 3, hence, we have to only consider the projection of the training data on features x_1, x_2 ignoring feature x_3 . This shows that problem $(\mathbf{P3}')$ is a special case of problem $(\mathbf{P4}')$. For instance, we can have a training dataset that have values for features x_1, x_2 generated based on the method used to prove $(\mathbf{P3}')$, while feature x_3 takes $x_3 = -1$ for all points that belong to class 0 and $x_3 = 1$ for all points that belong to class 1. It follows that problem $(\mathbf{P4}')$ is NP-hard.

D. Hardness of approximation

From the proof of $(\mathbf{P1}'), (\mathbf{P2}')$, we can see that a polynomial-time algorithm that approximates 2^{R_1} for problem $(\mathbf{P1}')$ or $(\mathbf{P2}')$ within $O(N^{1-\epsilon})$ for some $\epsilon > 0$ can be used to approximate the chromatic number within $O(N^{1-\epsilon})$ in polynomial time, since the chromatic number problem is polynomial-time reducible to problem $(\mathbf{P1}')$ or $(\mathbf{P2}')$ with $\mathcal{X}(G) = \min 2^{R_1}$, and number of

training points equal to the number of vertices in the graph. However, it was shown in [52] that approximating the chromatic number within $O(N^{1-\epsilon})$ is NP-hard $\forall \epsilon > 0$.

Similarly, from the proof of **(P3')**,**(P4')**, we can see that a polynomial-time algorithm that approximates 2^R for problem **(P3')** or **(P4')** within a factor of $O(N^{\frac{1}{2}-\epsilon})$ for some $\epsilon > 0$ can be used to approximate the BCBS within a factor of $O(N^{1-\epsilon})$ in polynomial time. The fraction $\frac{1}{2}$ in the exponent is because the BCBS problem is polynomial-time reducible to problem **(P3')** or **(P4')** with number of training points in the order of the square of the number of vertices in the graph. It was shown in [53] that approximating the BCBS within $O(N^{1-\epsilon})$ is NP-hard $\forall \epsilon > 0$ assuming the *Small Set Expansion Hypothesis* (SSEH) and that $\text{NP} \not\subseteq \text{BPP}$.

APPENDIX C

ON-THE-LINE OPTIMALITY

In this appendix, we prove the optimality of Algorithm 1 under the considered restriction (horizontal and vertical lines defining $d_{k,i}$ meet along the line $x_1 = x_2$) and assuming that the data points are linearly separable and scaled such that the line $x_1 = x_2$ separates the data.

We prove by induction that $\forall k \in [1 : 2N]$: at the k -th iteration of the algorithm, it finds the optimal quantization boundaries considering only the points $\mathcal{T}_{s_k} = \{(\mathbf{x}, y(\mathbf{x})) \in \mathcal{T} | x_1, x_2 \leq s_k\}$, $\forall b \in [1 : 2^R - 1]$, where s_k is the k -th smallest element in the set of possible boundaries \mathbf{s} .

- At the first iteration, there is only one possible position for all the boundaries, s_1 . Hence, at the first iteration the algorithm finds the optimal quantization boundaries considering the points \mathcal{T}_{s_k} , $\forall b \in [1 : 2^R - 1]$.
- Assuming that at iteration k the algorithm finds the optimal quantization boundaries considering the points \mathcal{T}_{s_k} , we show that it finds the optimal quantization boundaries considering the points $\mathcal{T}_{s_{k+1}}$ at iteration $k + 1$, $\forall b \in [1 : 2^R - 1]$.

At iteration $k + 1$, the only possible positions for the first boundary before s_{k+1} are the k positions s_1, s_2, \dots, s_k . Therefore, to find the optimal boundaries at iteration $k + 1$, we can condition on the position of the first boundary before s_{k+1} , and then optimize over this position. Conditioned on the position of the first boundary before s_{k+1} being at s_ℓ , the updated loss function can be expressed as

$$\mathcal{L}_{B \cup s_\ell}(\mathcal{E}, \mathcal{T}_{s_{k+1}}) = \mathcal{L}_B(\mathcal{E}, \mathcal{T}_{s_\ell}) + \min_{c \in \{1, 2\}} |\{j | s_\ell \prec \mathbf{x}^{(j)} \preceq s_{k+1}, y^{(j)} = c\}|, \quad (31)$$

where $\mathcal{L}_B(\mathcal{E}, \mathcal{T}_{s_\ell})$ is the loss $\mathcal{L}(\mathcal{E}, \mathcal{D}, \mathcal{T}_{s_\ell})$ when using the boundaries in the set B , and B is the set of boundaries in the region of the space defined by $\mathbf{x} \in \mathbb{R}^2 : \mathbf{x} \preceq s_\ell, |B \cup s_\ell| = b$.

This is, as we discussed in the paper, due to the fact that the misclassified points contributing to the quantizer loss can only lie in the 2-dimensional intervals crossed by the line $x_1 = x_2$. Which is because any other interval lies on one side of the line that separates the points, hence, contains points from only one class. Minimizing over all the possible values for s_ℓ, B we get

$$E(s_{k+1}, b) = \min_{B, \ell: |B| \leq b-1, \ell < k+1} \{ \mathcal{L}_B(\mathcal{E}, \mathcal{T}_{s_\ell}) + \min_{c \in \{1,2\}} |\{j | s_\ell \prec \mathbf{x}^{(j)} \preceq s_{k+1}, y^{(j)} = c\}| \}. \quad (32)$$

We can observe that only the first term in the previous minimization depends on B , hence, we can optimize over B first, which gives

$$E(s_{k+1}, b) = \min_{\ell < k+1} \left\{ E(s_\ell, b-1) + \min_{c \in \{1,2\}} |\{j | s_\ell \prec \mathbf{x}^{(j)} \preceq s_{k+1}, y^{(j)} = c\}| \right\}, \quad (33)$$

which is the update rule used in the algorithm. Hence, the boundaries corresponding to $E(s_{\ell^*}, b-1)$ along with the boundary at s_{ℓ^*} are the optimal boundaries at iteration $k+1$, where

$$\ell^* = \arg \min_{\ell < k+1} \left\{ E(s_\ell, b-1) + \min_{c \in \{1,2\}} |\{j | s_\ell \prec \mathbf{x}^{(j)} \preceq s_{k+1}, y^{(j)} = c\}| \right\}. \quad (34)$$

APPENDIX D

DISCUSSION ON BREAKING TIES IN GBI : THE PURITY CRITERION

In this section we illustrate what we call the purity criterion which is used to break ties in GBI. If it happens that two or more possible boundaries lead to the same quantizer loss (something that happened surprisingly often in our experiments), it makes a significant performance difference to add the boundary that looks ahead to allow future boundaries to further decrease the loss. The intuition behind this is the following: for a tie, we have a fixed number of misclassified points; what matters for the algorithm performance is that the misclassified points are in bins that can be more easily partitioned to bins that contains no misclassification in a next iteration. This was more likely to happen in our experiments (and small examples) if a bin that has misclassified points contained a number of majority class points that was just slightly higher than that of the misclassified classes. Formally, let H be an \mathbb{R}^n -bin and let \mathcal{T} be the set of training points $\{(\mathbf{x}^{(i)}, y(\mathbf{x}^{(i)}))\}$. Define, $B(H, \mathcal{T})$ as

$$B(H, \mathcal{T}) := \begin{cases} 0 & \text{if all points in } H \text{ are of the same class,} \\ \max_{c \in \mathcal{C}} |\{(\mathbf{x}, y(\mathbf{x})) \in \mathcal{T} \cap H \text{ s.t. } y(\mathbf{x}) = c\}| & \text{otherwise.} \end{cases}$$

$B(H, \mathcal{T})$ counts the number of points of the **majority** class in H when there is at least two or more classes represented in H , and is zero otherwise. For a particular set of boundaries that partition \mathbb{R}^n into the \mathbb{R}^n -bins $\{H_k\}_{k=1}^M$, we want to **minimize** the **purity criterion** defined as

$$U(\{H_k\}_{k=1}^M, \mathcal{T}) := \frac{\sum_{k=1}^M B(H_k, \mathcal{T})^2}{N},$$

where the term $B(H_k, \mathcal{T})^2$ penalizes bins with more majority points. $U(\{H_k\}_{k=1}^M, \mathcal{T})$ is minimized when the correctly classified points represent a weak majority in the bins that have misclassification. This allows for the bins that have misclassification to be easily partitioned to bins that have no misclassification in a following iteration. For illustration, consider the example shown in Figure 13. In this example all the potential boundaries ①, ②, ③, ④ result in the same value for the quantizer loss. However, it is clear that, unlike boundaries ③, ④, if we pick boundaries ①, ②, this allows for the separation of the “o” points (red) from the “x” points (blue) in the next iteration. The purity criterion chooses boundary ② as shown by the values in Figure 13. This choice separates the maximum number of “x” points from the bin that have misclassification. Note that, a power greater than 1, hence a function with slope that increases when we move away from zero, is needed in the purity criterion to highly penalize the bins that have misclassification having high concentration of majority class points, which prevents isolating the misclassified points in the following iterations. If we use a power of 1, the purity criterion is reduced to the quantizer loss. In our case we use a power of 2.

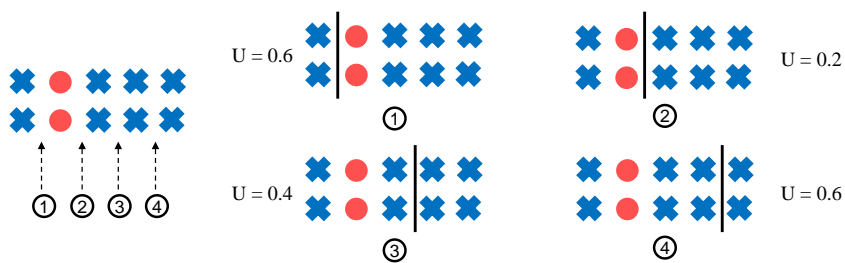


Fig. 13: Illustration of the purity criterion.

APPENDIX E

PARAMETERS OF TRAINED MODELS FOR EXPERIMENTAL EVALUATION

In this appendix, we describe the structure of the encoders/decoders neural networks and parameters used in the experimental results for each dataset.

A. sEMG dataset:

The structures of the neural networks used by the encoders $f_k(\cdot; \theta_k)$ and decoder $g(\cdot; \phi)$ are given in Table IV.

- **General parameters.** The distributed quantization system was trained using Adam optimizer with learning rate 10^{-3} for 300 epochs. The parameters of the pretrained classifier \mathcal{C} were frozen (not updated) during the learning phase.

TABLE IV: Structure of the encoder neural networks $f_k(\cdot; \theta_k)$ and the decoder neural network $g(\cdot; \phi)$ used for the sEMG dataset.

Encoder neural network $f_k(\cdot; \theta_k), \forall k \in [1 : 4]$			Decoder neural network $g(\cdot; \phi)$		
Layer Index	Layer Type	Output size	Layer Index	Layer Type	Output size
1	FC-Relu	90	1	FC-Relu	170
2	FC-Relu	170	2	FC-Relu	90
3	FC-Batchnorm-Tanh	# of bits per encoder	3	FC	8

- **NN-REG.** For our approach in Section VI-A, we chose the regularization parameter β through 5-fold cross validation out of possible parameter values $\{0, 0.1, \dots, 2\}$. The chosen regularization parameter is $\beta = 1.4$.

- **NN-GBI.** For our approach in Section VI-B, the output of the last layer in the encoder was chosen to be 1 when applying **Phase 1** (refer to Section VI-B). When applying GBI, a batch size of 300 data points was used in each iteration of the GBI algorithm. After designing the quantizer with GBI, the network is trained for an extra 20 epochs with the quantizer in **Phase 3**.

B. CIFAR10 dataset:

The structures of the neural networks used by the encoders $f_k(\cdot; \theta_k)$ and decoder $g(\cdot; \phi)$ are given in Table V and Table VI, respectively.

- **General parameters.** The distributed quantization system was trained using Adam optimizer with learning rate 10^{-3} for 200 epochs. The parameters of the pretrained classifier \mathcal{C} were frozen (not updated) during the learning phase.

- **NN-REG.** The chosen regularization parameter is $\beta = 0.25$.
- **NN-GBI.** For our approach in Section VI-B, the output of the last layer in the encoder was chosen to be 5 when applying **Phase 1** (refer to Section VI-B). When applying GBI, a batch size

of 300 data points was used in each iteration of the GBI algorithm. After designing the quantizer with GBI, the network is trained for an extra 50 epochs with the quantizer in **Phase 3**.

TABLE V: Structure of encoder neural networks $f_k(\cdot; \theta_k)$ used for CIFAR-10 dataset.

Layer Index	Layer Type	Output size	Input channels	Output channels	Kernel size	Stride	Padding
1	Conv-Relu	-	3	64	3	1	1
2	Conv-Relu	-	64	64	3	1	1
3	Maxpool	-	-	-	2	2	-
4	Conv-Relu	-	64	128	3	1	1
5	Conv-Relu	-	128	128	3	1	1
6	Maxpool	-	-	-	2	2	-
7	FC-Tanh	number of bits per encoder	-	-	-	-	-

TABLE VI: Structure of decoder neural network $g(\cdot; \phi)$ used for CIFAR-10 dataset.

Layer Index	Layer Type	Output size	Input channels	Output channels	Kernel size	Stride	Padding
1	FC-Relu	80	-	-	-	-	-
2	ConvTranspose-Relu-Batchnorm	-	5	5	4	2	1
3	ConvTranspose-Relu-Batchnorm	-	5	5	4	2	1
4	ConvTranspose-Relu-Batchnorm	-	5	5	4	2	1
5	Conv	-	5	3	5	1	2

REFERENCES

- [1] A. Courville and I. G. and Yoshua Bengio, *Deep learning*. MIT press, 2015.
- [2] M. A. Lebedev and M. A. Nicolelis, “Brain–machine interfaces: past, present and future,” *TRENDS in Neurosciences*, vol. 29, no. 9, 2006.
- [3] “Google Cloud AI,” <http://cloud.google.com/products/ai/>, 2008, [Online; accessed 19-July-2008].
- [4] “Clarifai,” <http://clarifai.com/>.
- [5] A. van den Oord, O. Vinyals, and K. Kavukcuoglu, “Neural discrete representation learning,” in *Advances in Neural Information Processing Systems*, 2017, pp. 6306–6315.
- [6] A. Razavi, A. van den Oord, and O. Vinyals, “Generating diverse high-fidelity images with VQ-VAE-2,” *arXiv preprint arXiv:1906.00446*, 2019.
- [7] K. Choi, K. Tatwawadi, T. Weissman, and S. Ermon, “NECST: neural joint source-channel coding,” *arXiv preprint arXiv:1811.07557*, 2018.
- [8] L. Theis, W. Shi, A. Cunningham, and F. Huszár, “Lossy image compression with compressive autoencoders,” *arXiv preprint arXiv:1703.00395*, 2017.
- [9] J. Ballé, V. Laparra, and E. P. Simoncelli, “End-to-end optimization of nonlinear transform codes for perceptual quality,” in *2016 Picture Coding Symposium (PCS)*. IEEE, 2016, pp. 1–5.
- [10] A. Van Oord, N. Kalchbrenner, and K. Kavukcuoglu, “Pixel recurrent neural networks,” in *International Conference on Machine Learning*, 2016, pp. 1747–1756.
- [11] J.-F. Chamberland and V. V. Veeravalli, “Wireless sensors in distributed detection applications,” *IEEE Signal Processing Magazine*, vol. 24, no. 3, pp. 16–25, 2007.
- [12] Z.-Q. Luo, “Universal decentralized estimation in a bandwidth constrained sensor network,” *IEEE Transactions on Information Theory*, vol. 51, no. 6, pp. 2210–2219, 2005.
- [13] M. Longo, T. D. Lookabaugh, and R. M. Gray, “Quantization for decentralized hypothesis testing under communication constraints,” *IEEE Trans. on Inf. Theory*, vol. 36, no. 2, pp. 241–255, 1990.
- [14] T. S. Han and S. Amari, “Statistical inference under multiterminal data compression,” *IEEE Transactions on Information Theory*, vol. 44, no. 6, pp. 2300–2324, Oct 1998.
- [15] Y. Han, A. Özgür, and T. Weissman, “Geometric lower bounds for distributed parameter estimation under communication constraints,” in *The 31st Annual Conference on Learning Theory*, 2018.
- [16] I. Diakonikolas, E. Grigorescu, J. Li, A. Natarajan, K. Onak, and L. Schmidt, “Communication-efficient distributed learning of discrete distributions,” in *Advances in Neural Information Processing Systems*, 2017, pp. 6391–6401.
- [17] J. Acharya, C. L. Canonne, and H. Tyagi, “Distributed simulation and distributed inference,” *arXiv preprint arXiv:1804.06952*, 2018.
- [18] H. V. Poor, “High-rate vector quantization for detection,” *IEEE Transactions on Information Theory*, vol. 34, p. 960972, 1988.
- [19] J. Z. Sun, V. Misra, and V. K. Goyal, “Distributed functional scalar quantization simplified,” *IEEE Transactions on Signal Processing*, vol. 61, no. 14, pp. 3495–3508, 2013.
- [20] V. Misra, V. K. Goyal, and L. R. Varshney, “Distributed scalar quantization for computing: High-resolution analysis and extensions,” *IEEE Transactions on Information Theory*, vol. 57, no. 8, pp. 5298–5325, 2011.
- [21] T. Kohonen, J. Hynninen, J. Kangas, J. Laaksonen, and K. Torkkola, “Lvc pak: The learning vector quantization program package,” Technical report, Laboratory of computer and Information Science , Tech. Rep., 1996.

- [22] A. Sato and K. Yamada, "Generalized learning vector quantization," in *Advances in neural information processing systems*, 1996, pp. 423–429.
- [23] T. Berger, Z. Zhang, and H. Viswanathan, "The ceo problem [multiterminal source coding]," *IEEE Transactions on Information Theory*, vol. 42, no. 3, pp. 887–902, 1996.
- [24] H. Viswanathan and T. Berger, "The quadratic gaussian ceo problem," *IEEE Transactions on Information Theory*, vol. 43, no. 5, pp. 1549–1559, 1997.
- [25] Y. Oohama, "The rate-distortion function for the quadratic gaussian ceo problem," *IEEE Transactions on Information Theory*, vol. 44, no. 3, pp. 1057–1070, 1998.
- [26] V. Prabhakaran, D. Tse, and K. Ramachandran, "Rate region of the quadratic gaussian ceo problem," in *International Symposium on Information Theory, 2004. ISIT 2004. Proceedings.* IEEE, 2004, p. 119.
- [27] A. B. Wagner, "On distributed compression of linear functions," *IEEE Transactions on Information Theory*, vol. 57, no. 1, pp. 79–94, 2011.
- [28] D. Krithivasan and S. S. Pradhan, "Lattices for distributed source coding: Jointly gaussian sources and reconstruction of a linear function," *IEEE Transactions on Information Theory*, vol. 55, no. 12, pp. 5628–5651, 2009.
- [29] V. Doshi, D. Shah, M. Médard, and M. Effros, "Functional compression through graph coloring," *IEEE Transactions on Information Theory*, vol. 56, no. 8, pp. 3901–3917, 2010.
- [30] A. Zhou, A. Yao, Y. Guo, L. Xu, and Y. Chen, "Incremental network quantization: Towards lossless cnns with low-precision weights," in *International Conference on Learning Representations*, 2017.
- [31] B. Jacob, S. Kligys, B. Chen, M. Zhu, M. Tang, A. Howard, H. Adam, and D. Kalenichenko, "Quantization and training of neural networks for efficient integer-arithmetic-only inference," in *Proceedings of the IEEE Conference on Computer Vision and Pattern Recognition*, 2018, pp. 2704–2713.
- [32] S. Wu, G. Li, F. Chen, and L. Shi, "Training and inference with integers in deep neural networks," in *International Conference on Learning Representations*, 2018.
- [33] W. Gao, Y.-H. Liu, C. Wang, and S. Oh., "Rate distortion for model compression: From theory to practice," in *ICML*, 2019, pp. 2102–2111.
- [34] Y. Freund and R. E. Schapire, "A decision-theoretic generalization of on-line learning and an application to boosting," *Journal of computer and system sciences*, vol. 55, no. 1, pp. 119–139, 1997.
- [35] T. Hastie, S. Rosset, J. Zhu, and H. Zou, "Multi-class adaboost," *Statistics and its Interface*, vol. 2, no. 3, pp. 349–360, 2009.
- [36] Z. Tu, P. Dollar, and Y. Wu, "Layered logic classifiers: Exploring theand'andor'relations," *arXiv preprint arXiv:1405.6804*, 2014.
- [37] D. P. Kingma and M. Welling, "Auto-encoding variational bayes," *arXiv preprint arXiv:1312.6114*, 2013.
- [38] I. Higgins, L. Matthey, A. Pal, C. Burgess, X. Glorot, M. Botvinick, S. Mohamed, and A. Lerchner, "beta-vae: Learning basic visual concepts with a constrained variational framework." *ICLR*, vol. 2, no. 5, p. 6, 2017.
- [39] S. Zhao, J. Song, and S. Ermon, "Infovae: Balancing learning and inference in variational autoencoders," in *Proceedings of the AAAI Conference on Artificial Intelligence*, vol. 33, 2019, pp. 5885–5892.
- [40] E. Mathieu, T. Rainforth, N. Siddharth, and Y. W. Teh, "Disentangling disentanglement in variational autoencoders," in *International Conference on Machine Learning*, 2019, pp. 4402–4412.
- [41] A. Alemi, I. Fischer, J. Dillon, and K. Murphy, "Deep variational information bottleneck," in *ICLR*, 2017.
- [42] N. Tishby, F. C. Pereira, and W. Bialek, "The information bottleneck method," *arXiv preprint physics/0004057*, 2000.
- [43] J. Munkres, *Topology*. Pearson Education, 2014.
- [44] C. M. Bishop, *Pattern recognition and machine learning*. springer, 2006.

- [45] M. Shohat, G. Tsintsadze, N. Shlezinger, and Y. C. Eldar, "Deep quantization for mimo channel estimation," in *ICASSP 2019-2019 IEEE International Conference on Acoustics, Speech and Signal Processing (ICASSP)*. IEEE, 2019, pp. 3912–3916.
- [46] B. C. Csáji, "Approximation with artificial neural networks," *Faculty of Sciences, Eötvös Loránd University, Hungary*, vol. 24, p. 48, 2001.
- [47] S. Lobov, N. Krilova, I. Kastalskiy, V. Kazantsev, and V. Makarov, "Latent factors limiting the performance of sEMG-interfaces," *Sensors*, vol. 18, no. 4, p. 1122, 2018.
- [48] J. MacQueen, "Some methods for classification and analysis of multivariate observations," in *Proceedings of the fifth Berkeley symposium on mathematical statistics and probability*, vol. 1, no. 14. Oakland, CA, USA, 1967, pp. 281–297.
- [49] K. Simonyan and A. Zisserman, "Very deep convolutional networks for large-scale image recognition," in *ICLR*, 2015.
- [50] R. M. Karp, "Reducibility among combinatorial problems," in *Complexity of computer computations*. Springer, 1972, pp. 85–103.
- [51] N. Alon, R. A. Duke, H. Lefmann, V. Rodl, and R. Yuster, "The algorithmic aspects of the regularity lemma," *Journal of Algorithms*, vol. 16, no. 1, pp. 80–109, 1994.
- [52] D. Zuckerman, "Linear degree extractors and the inapproximability of max clique and chromatic number," in *Proceedings of the thirty-eighth annual ACM symposium on Theory of computing*. ACM, 2006, pp. 681–690.
- [53] P. Manurangsi, "Inapproximability of maximum edge biclique, maximum balanced biclique and minimum k-cut from the small set expansion hypothesis," in *44th International Colloquium on Automata, Languages, and Programming (ICALP 2017)*. Schloss Dagstuhl-Leibniz-Zentrum fuer Informatik, 2017.